RESEARCH ON DIGITAL

TRANSDUCER PRINCIPLES

VOLUME III

CHARGE TRANSPORT MECHANISMS IN THIN

POLYMER FILMS

for the

NATIONAL AERONAUTICS AND SPACE ADMINISTRATION

GRANT NGR 44-012-043

Covering the Period

July 1, 1966 - June 30, 1967

by

Eugene T. Fitzgibbons

William H. Hartwig

The University of Texas

Austin, Texas 78712

ABSTRACT

Electron currents between metal electrodes separated by an
insulator can be explained on the basis of field (tunneling) or ther-
mal emission. Analytical expressions, based on a band-gap model of
the insulator, have been derived and exist in the literature. These
expressions are, in general, explicit in the electrical properties of
the insulator, the physical configuration of the junction and the ex-
ternal conditions such as applied bias, temperature, etc.

Experiments were conducted on metal-insulator-metal junctions
to determine the characteristics and develop, to a certain degree
of sophistication, the technology of thin film devices. The junctions
consisted of Al electrodes separated by a thin polymer film. The film
was formed by polymerizing silicone diffusion pump oil, incident on
the junction substrate with an electron beam. Although this polymer
is rather an amorphous material when compared with the periodic struc-
ture of some insulating materials, it is assumed that the familiar
band gap model is still valid and useful.

The voltage-current characteristics of the devices are highly
dependent on insulator thickness. Some hysteresis is observed at low
fields. Evidence for the formation of a polarization charge is seen.
The junctions are quite symmetrical in their electrical behavior.

The experimental voltage-current curves are understandable
in the light of tunneling theory. For thicker samples, evidence is
found that indicated that field and thermal current mechanisms operate
simultaneously. Sharp breaks in the slopes of the V-I curves can be

explained by postulating that field emission becomes the more dominant
mechanism as the applied bias is increased.

The slope and zero bias intercepts of the current-voltage
curves yield data about the insulator. The dielectric constant at
1 kc is 2.8 and the index of refraction is 1.5. The barrier height
at zero bias is ϕ_0 = 1.05 ev. The effective mass of an electron in
the forbidden band of the insulator is 0.11 m_e.

TABLE OF CONTENTS

LIST OF FIGURES

CHAPTER I

THEORY OF METAL-INSULATOR-METAL CURRENT MECHANISMS

A.   Introduction

Current flowing between two metal electrodes separated by

an insulating barrier can be explained on the basis of either or both

of two mechanisms. At 0°K and under the influence of a high electric

field, electron currents are understandable only in the light of quan-

tum mechanical field emission. At temperatures above 0°K and with

no bias applied, thermal emission accounts for any current flowing.

Various special cases of both mechanisms have been studied in some

detail and will be considered below.

These mechanisms are all based on a band gap model of the

insulating layer. This model is quite agreeable when considering in-

sulating solids in the crystalline state. However, where the substance

is not crystalline but amorphous, assertions based solely on the sim-

ple Kronig-Penney model are no longer valid.

Although a long range order does not exist in amorphous sub-

stances, a certain amount of short range ordering is found. This short

range order indicates the presence of atom-atom interactions. If the

component atoms are "brought in" from infinity to their respective po-

sitions in the amorphous material, the degeneracy of the atomic levels

in the individual atoms is removed by the mutual interaction, with the

result that each highly degenerate level is still split into a large

number of distinct levels. These levels may not be as numerous as

those in a crystalline substance but exist in sufficient quantities

1

to define energy bands. For amorphous insulators such as polymers, composed of large and irregular molecules, the band gap and the density of states in the valence and conduction bands are, presumably, functions of position in the "quasi" lattice. It is understandable that, for this type of material, average values for the band gap must be adopted.

B. Field Emission

The wave-particle duality of the electron may be expressed by Schrodinger's time independent equation which describes the motion of an electron as a wave packet moving through three dimensional space. This relation may be written in the form

$$\frac{-h^2}{2m} \nabla^2 u - (E - eV)u = 0 \tag{1}$$

Various solutions to this equation are undertaken in Leighton[1], Messiah[2] and others[3,4]. One of the most important cases of the above is that of a "one-dimensional" free-particle encountering a potential barrier. It is found[1,2,3,4] that as a result of the impact with a barrier whose height is too great, at least classically, for the particle to surmount, there is a finite probability the particle will penetrate into and beyond the barrier. The solution to equation (1) inside the barrier is a wave whose amplitude dies off exponentially. This exponential decay can be thought of as a transmission coefficient which may be written, with the help of the well known WKB approximation as

$$D(E) = \exp \frac{-4\pi}{h} \int_{s_1}^{s_2} [2m(V(x) - E_x)]^{1/2} dx \tag{2}$$

where $E_x = 1/2\ mv_x^2$ and s_1 and s_2 are as shown in figure 1.
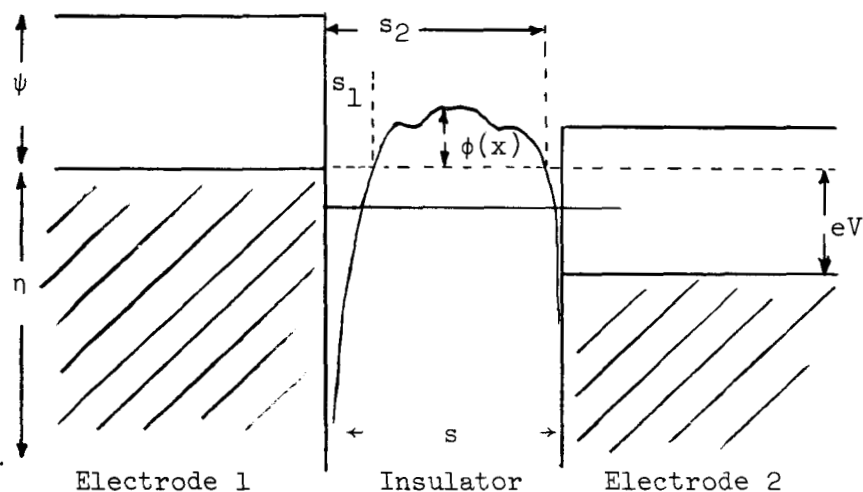
Figure 1

General Barrier in an Insulating Film Between Two Metal Electrodes

The quantity $D(E_x)$ may be interpreted as the probability that any given electron, incident on the metal-insulator boundary, will be transmitted through the insulator. The current of electrons successfully tunneling through the barrier is written, in differential form

$$dJ_x = ev_x \, D(E_x)dN \qquad (3)$$

J_x = current density in the x direction

$e = 1.6 \times 10^{-19}$ coul.

v_x = velocity in the x direction corresponding to E_x

$D(E_x)$ = transmission coefficient.

Following the method of Simmons[5] and integrating equation (3), the current from electrode 1 collected by electrode 2 may be

written

$$J_1 = e \int_o^{v_m} v_x \, n(v_x)D(E_x)dv_x = \frac{e}{m} \int_o^{E_m} n(v_x)D(E_x)dE_x \qquad (4)$$

where

$n(v_x)dv_x$ = density of electrons with x component of velocity

between v_x and $v_x + dv_x$

v_m, E_m = the maximum x directed velocity/energy in the

electrode.

For an isotropic velocity distribution in the electrode, the density of electrons is

$$n(v_x,v_y,v_z)dv_x dv_y dv_z = \frac{2m^4}{h^3} f(E)dv_x dv_y dv_z \qquad (5)$$

where $f(E)$ is the Fermi-Dirac distribution function. It is a fact that, for any probability density function of several independent variables, the density function of a subset of the variables may be written[31]

$$g(a) = \int_{-\infty}^{\infty} g(a,b,c)dbdc$$

In this fashion

$$n(v_x)dv_x = \frac{2m^4}{h^3} dv_x \int_{-\infty}^{\infty} f(E)dv_y dv_z \qquad (6a)$$

or

$$n(v_x) = \frac{4\pi m^3}{h^3} \int_o^{\infty} f(E)dE_r \qquad (6b)$$

where

$$E_r = 1/2 \ m(v_y^2 + v_z^2) = 1/2 \ mv_r^2$$

Using this fact, equation (4) can now be written as

$$J_1 = \frac{4\pi m^2 e}{h^3} \int_0^{E_m} D(E_x)dE_x \int_0^\infty f(E)dE_r \qquad (7)$$

The flow of electrons away from electrode 2, biased at V above electrode 1, is similar in form.

$$J_2 = \frac{4\pi m^2 e}{h^3} \int_0^{E_m} D(E_x)dE_x \int_0^\infty f(E + eV)dE_r \qquad (8)$$

The net current is

$$J = J_1 + J_2$$

$$= \frac{4\pi m^2 e}{h^3} \int_0^{E_m} D(E_x)dE_x \int_0^\infty [f(E) - F(E + eV)]dE_r \qquad (9)$$

Up to this point, tunneling theory is quite straightforward and uniform from author to author. However, to perform the integration of the transmission coefficient it is necessary to make approximations about the shape of the tunneling barrier and decide on "representative" parameters for non-uniform or difficult shapes.

Fowler and Nordheim[6] and Holms[7] calculate the current for a simple rectangular barrier and Holms includes a correction term for the image force that a charge experiences when it is in the proximity of a metal plate. More recent work by Simmons[5,8,9] and Stratton[10]

includes the above work and adds several important refinements. It
is worthwhile to consider the results of Simmons and then Stratton.

Simmons begins by writing $V(x) = \eta + \phi(x)$ as in figure 1.
Equation 2 becomes

$$D(E_x) = \exp \frac{-4\pi}{h}(2m)^{1/2} \int_0^s [\eta + \phi(x) - E_x]^{1/2}dx \quad (10)$$

where s is the thickness of the insulator. For any type of barrier,
it is convenient to define the mean barrier height $\bar{\phi}$ with reference
to the Fermi level of the negatively biased electrode.

$$\bar{\phi} = \frac{1}{s} \int_0^s \phi(x)dx \quad (11)$$

Using equations (10) and (11), Simmons[5] integrates equation (9)
with the following result:

$$J_x = \frac{E}{2\pi hs^2} \{\bar{\phi} \exp[-\frac{e}{2\pi hs^2} (\bar{\phi})^{1/2}]$$

$$-(\bar{\phi} + eV) \exp[-\frac{e}{2\pi hs^2} (\bar{\phi} + eV)^{1/2}] \} \quad (12)$$

At this point the alteration of the barrier shape due to the
image force must be considered. As an electron leaves the cathode of
the tunneling junction it is acted on by its image charge on the face
of the electrode. This interaction is one of attraction and alters the
potential map to a large extent at that barrier edge. Actually, the
tunneling charge does not "see" a single image charge but is acted on
by an infinite series of image charges, i.e., the image of the image
in the second electrode and so forth. The image potential due to

this series of charges is[32]

$$V_i = \left(\frac{-e^2}{4\pi\varepsilon}\right) \left\{ \frac{1}{2x} + \sum_{n=1}^{\infty} \left[\frac{ns}{n^2s^2-x^2} - \frac{1}{ns} \right] \right\} \qquad (13)$$

where x is the distance of the electron from electrode 1. A good approximation to equation (13) is given by Simmons (reference 5, equation 33). This approximation may be written

$$V_i = \frac{-e^2}{4\pi\varepsilon} \left\{ \frac{1.15\ell n2}{2} \quad \frac{1}{s} \quad \frac{s^2}{x(s-x)} \right\}$$

or

$$V_i = \frac{-1.15\lambda s^2}{x(s-x)} \qquad (14)$$

where

$$\lambda = \frac{e^2 \ell n2}{8\pi\varepsilon s}$$

If the image potential and the potential due to an external bias, V_1, is considered, the total potential of an electron in the insulator is

$$\phi(x) = \phi_o - \frac{eVx}{s} - \frac{1.15\lambda s^2}{x(s-x)} \qquad (15)$$

The effective thickness of the barrier is determined by the real roots of the above equation. These roots represent the points where the electron potential is zero with respect to the Fermi level of electrode 1.

The applied bias may be in three different ranges

$$eV = 0$$

$$eV < \phi_o$$

$$eV > \phi_o$$

The last case is, in general, the case anticipated in the experimental work. For this case, the roots to equation (15) may be written to good approximation

$$s_1 = 1.2\lambda s/\phi_o$$

$$s_2 = (\phi_o - 5.6\lambda)(s/eV) \tag{16}$$

The corrected barrier height, ϕ_I, may be found by replacing the integral in equation (11) with equation (15) and changing the limits of integration to s_1 and s_2.

Performing the integration, it is found that

$$\phi_I = \phi_o - \frac{eV}{2s}(s_1 + s_2) - \left(\frac{1.15\lambda s}{s_2 - s_1}\right)\ln\left[\frac{s_2(s-s_1)}{s_1(s-s_2)}\right] \tag{17}$$

Figure 2a shows the three possible bias levels with no image force correction. Figure 2b shows the same bias conditions with the image force taken into consideration. It is seen that the mean barrier height for the image corrected barrier is smaller than that for the uncorrected barrier for corresponding bias conditions.

Using these corrected parameters, equation (12), as given by Simmons[10], may be rewritten as

$$J_x = \frac{e}{2\pi h(\Delta s)^2} \left\{ \phi_I \exp\left[- \frac{E}{2\pi h(\Delta s)^2}(\phi_I)^{1/2}\right] \right.$$

$$\left. + (\phi_I + eV) \exp\left[- \frac{e}{2\pi h(\Delta s)^2}(\phi_I + eV)^{1/2}\right] \right\} \tag{18a}$$
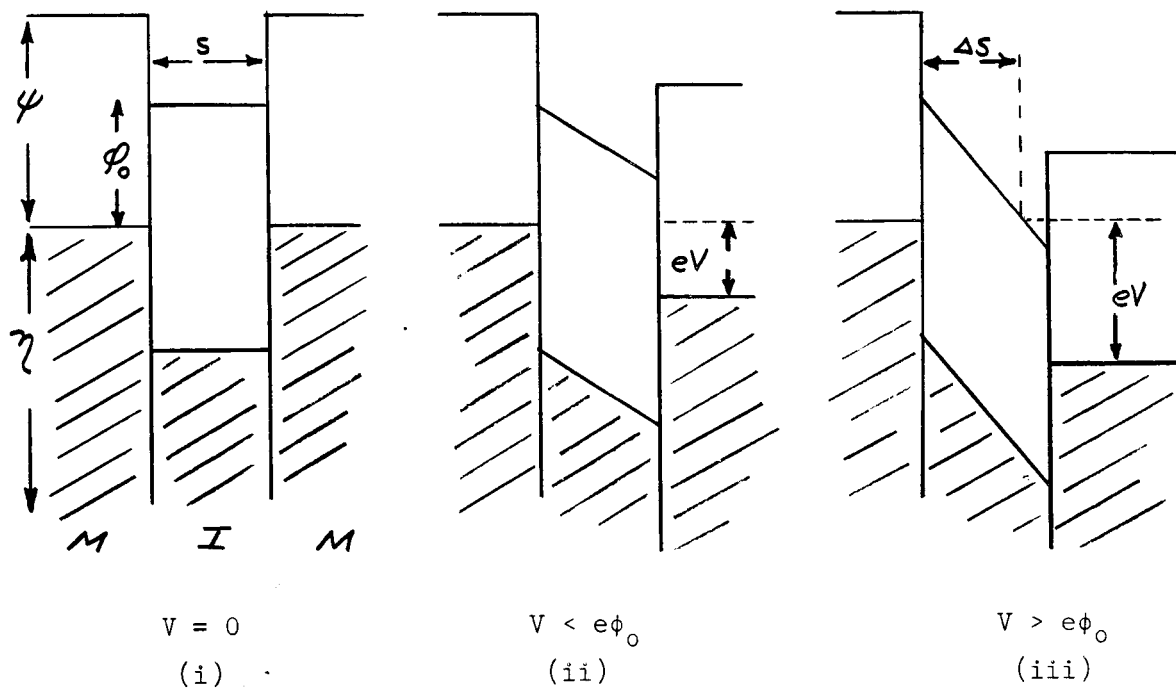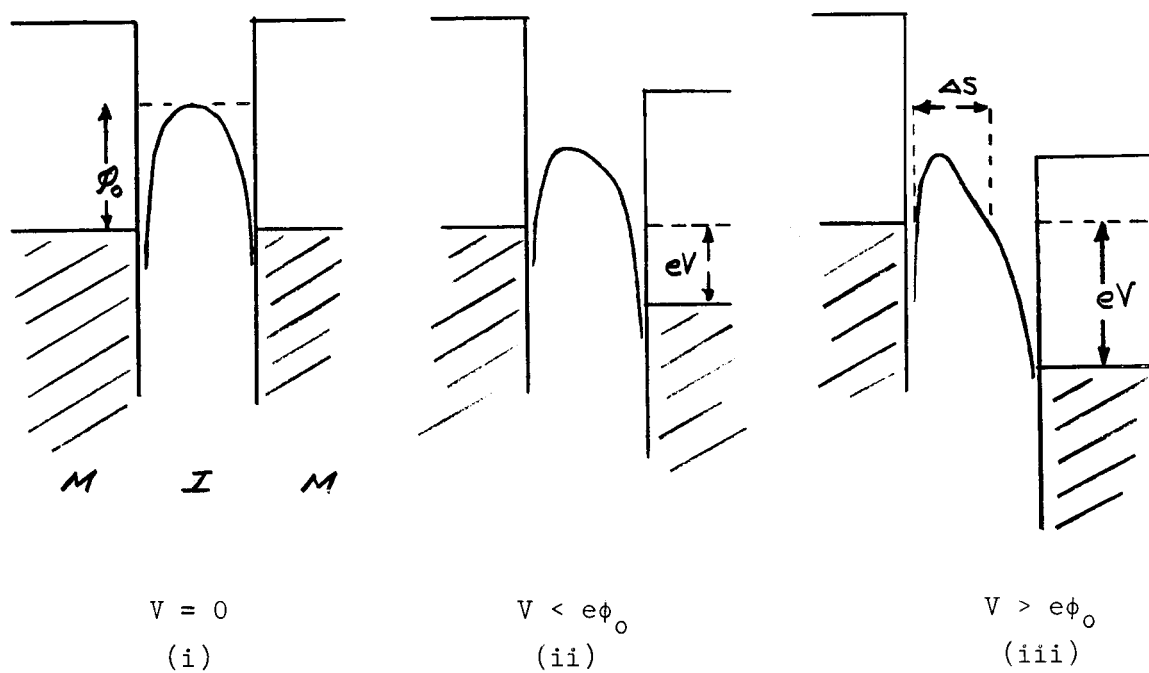
Figure 2a

Figure 2b

Insulating Barrier as a Function of Applied Bias

or, in practical units

$$J_x = \frac{6.2 \times 10^{10}}{(\Delta s)^2} \{\phi_I \exp(-1.025\Delta s \phi_I^{1/2}) - (\phi_I + V) \times$$

$$\exp[-1.025 \; \Delta s(\phi_I + V)^{1/2}] \} \tag{18b}$$

where Δs is in angstroms, ϕ_I in e-volts, V in volts and J in amps/cm^2

Stratton replaces the transmission coefficient expressed in equation (2) by an infinite series and then retains only the linear term in E_x such that

$$\log D \simeq -[b_1 + c_1 (\eta - E_x)] \tag{19}$$

where

$$b_1 = \frac{4\pi(2m)^{1/2}}{h} \int_{s_1}^{s_2} [\phi(x)]^{1/2} dx$$

and

$$c_1 = \frac{2\pi(2m)^{1/2}}{h} \int_{s_1}^{s_2} [\phi(x)]^{-1/2} dx \tag{20}$$

The points s_1 and s_2 are the same as those given by equation (16) and represent the points where $\phi(x) = 0$ with respect to the Fermi level, η, of the negative electrode. Stratton carries out the integration of equation (9) using the method of Murphy and Good[11] and the above approximation to obtain the following equation:

$$J = [\frac{4\pi em(kT)^2}{h^3}] \frac{\pi c_1 kT}{(c_1 kT)^2 \sin(\pi c_1 kT)} [\exp(-b_1)] \times$$

$$[1 - \exp(-c_1 V)] \tag{21}$$

In effect, what Stratton has done is to replace the true potential barrier potential $\phi(x)$ by a rectangular barrier where height ϕ_r is so determined that

$$\phi_r = \{\frac{1}{\Delta s} \int_{s_1}^{s_2} [\phi(x)]^{1/2} dx \}^2 \tag{22}$$

That is, ϕ_r is the square of the average value of $[\phi(x)]^{1/2}$. This quantity is quite different than $\bar{\phi}$ as defined by equation (11).

From (21) Stratton derives the current density expression for a symmetric barrier as

$$J = \frac{4\pi me(kT)^2}{h^2} \frac{\pi c_{10} kT \exp(b_{10})}{(c_{10} kT)^2 \sin(\pi c_1 kT)} \exp(-b_{12} V^2) \sinh(\frac{c_{10}}{2} eV)$$

$$= \frac{A\pi}{c_{10} kT} \frac{\exp(-b_{10})}{\sin(\pi c_{10} kT)} \exp(-b_{12} V^2) \sinh(\frac{c_{10}}{2} eV) \tag{23}$$

where the b's and c's are coefficients of b_1 and c_1 expressed as power series in V. The series are

$$b_1 = b_{10} - b_{11} V + b_{12} V^2 + \ldots$$

$$\tag{24}$$

$$c_1 = c_{10} - c_{11} V + c_{12} V^2 + \ldots$$

With a reasonable amount of accuracy, depending on the voltage range, only the first three terms in the expansion for b_1 and the first term

in c_1 need to be retained. Although this appears to be a rather arbitrary step, good agreement with experimental data at low to moderate voltages is obtained. At most bias voltages encountered in the following experiments a good approximation to equation (23) is:

$$J = \frac{AI_0}{2} \exp(-b_{12}V^2) \exp(\frac{c_{10}}{2} eV) \qquad (25)$$

where $I_0 = \frac{\pi}{c_{10}kT} \frac{\exp(-b_{10})}{\sin(\pi c_{10}kT)}$

The factor of e in the argument of the second exponent was not included in the original paper (ref. 10).

It is important to note that although c_{10} and b_{12} are coefficients of a series expansion, they have not lost their identity with the parameters of the physical system but may easily be found from equation (19) by expanding $[\phi(x,V)]^{1/2}$ as a series in V and integrating.

The temperature dependence of the tunneling phenomenon may be obtained from equation (21). If the voltage is held constant, the current through the sample may be written as

$$J(V = const.) = \frac{J(0)kT\pi c_{10}}{\sin(\pi c_{10}kT)} \qquad (26)$$

where $J(0) = \frac{4\pi me}{h^2} \frac{\exp(b_{10})}{c_{10}}$

Expanding the sine term in the denominator

$$J(V = \text{const.}) = J(0)[1 + 1/6(\pi c_{10} kT)^2 + \ldots] \qquad (27)$$

or

$$J(V = \text{const.}) - J(0) = \alpha T^2$$

This temperature dependence results from either Stratton or Simmons'
equation.

C. Thermal Emission

The Fermi-Dirac distribution predicts that, out of a large
group of electrons, a certain number will posses energies higher than
a given value. With respect to a metal-insulator interface, this im-
plies that a number of electrons in the electrode will have sufficient
energy to pass directly into the conduction band of the insulator and
be collected by a second electrode. For a metal-vacuum interface the
current of these electrons is given by the Richardson equation[30].

$$J = \frac{1}{(2\pi)^2} \frac{2em(kT)^2}{h^3} \exp \frac{-\psi}{kT} \qquad (28)$$

where ψ is the work function of the electrode.

For emission into an insulator other than a vacuum, equation
(28) should be modified in two ways. First, the electron in the in-
sulator is not free but, constrained by the insulator conduction band,
necessitating the definition of an effective mass, m^*, for the elec-
tron in this region. Second, the metal-insulator potential boundary
must be modified to include the image force experienced by the elec-
tron in the insulator while still in the proximity of the electrode.
Taking both of these points into consideration, Johnson[12] writes the

thermal current as

$$J = (\frac{1}{2\pi})^2 \; \frac{2em^*}{h^3} \; (kT)^2 \; \exp \frac{-\phi}{kT} \; \exp \; [\frac{e^3F}{4\pi K\epsilon o}]^{1/2} \qquad (29)$$

where K = relative dielectric constant of the insulator

F = electric field in the insulator, V/s.

Taking the log of both sides of equation (24), it is apparent that

$$\ln \; J \propto T$$

Since thermal or Schottky emission, unlike tunneling, is exponentially dependent on temperature, it is often advantageous to use a variation in temperature to identify and separate mechanisms.

D. Summary of Theory

The above summation of field and thermal emission theory allows several important conclusions to be drawn which are directly applicable to the subsequent discussion of experimental results.

a) Simmons' equation (18) expresses the tunneling current explicitly in terms of the "corrected" physical parameters of the system.

b) By considering the image forces and the external bias, the dielectric thickness and the barrier height may be assigned corrected or effective values. These effective parameters are explicit functions of the uncorrected values, the dielectric constant and the applied bias.

c) Stratton's equation (23) involves approximations yet remains explicit in the junction parameters. Because of its relative simplicity, the equation lends itself to

comparison with theory.

d) Both theoretical formulations lead to

    i) the Sommerfield-Bethe or Fowler-Nordheim equation as the bias becomes much larger than the barrier height.

    ii) a T^2 dependence of current on temperature at a constant bias.

e) The thermal component of the current in the dielectric is given by the Schottky equation (29). This equation predicts an exponential temperature dependence and suggests ways of measuring the system parameters.

CHAPTER II

EXPERIMENTAL METHOD

A. Introduction

Metal-insulator-metal junctions in which the insulator thickness
is on the order of 100 $\overset{o}{A}$ or less, yet is uniformly thick and free of cata-
strophic defects such as pinholes and shorts, require well developed
technology to produce and a certain amount of experimental sophistica-
tion to test. In order to measure very small currents through the sample
(on the order of 10^{-9} to 10^{-12} amps) with good precision, circuits with
minimum noise and maximum stability had to be engineered. Much care was
taken to keep the effect of unknown parameters at a minimum.

B. The Tunneling Junction

1. Metal-Insulator-Metal Configuration

Figure 4 shows the basic, physical configuration of the
metal-insulator-metal (MIM) junction. The metal electrodes are at right
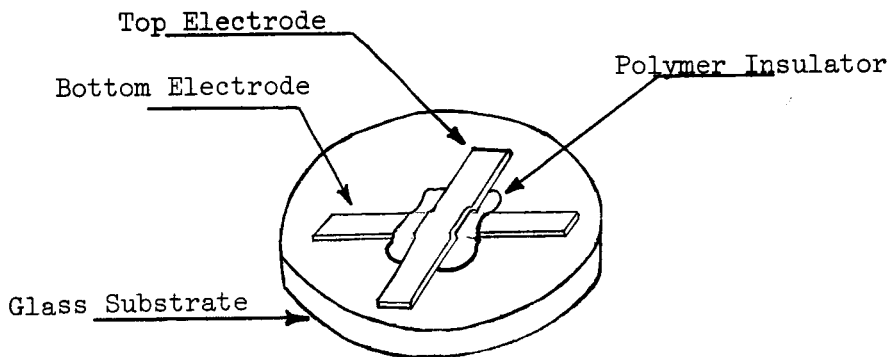
Figure 3

Basic MIM Configuration

angles to each other, separated at their overlap by a polymer insulator
and extending approximately 1 cm. beyond the junction to provide electrical
contact for testing. Samples of this configuration were especially easy
to connect to, and, for this reason, gave quite consistent data.
However, only one sample of this type could be made per run, often con-
suming several hours. A second configuration, figure 5, allows three
junctions to be made at a time. It was found, though, that difficulties
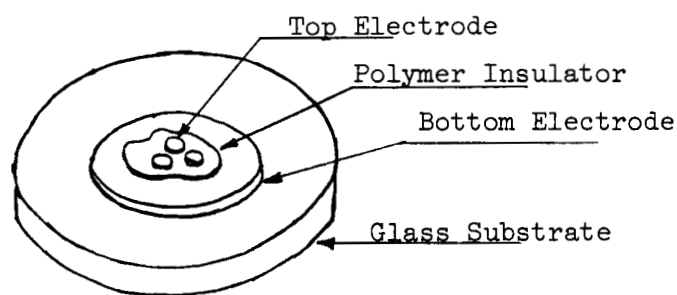
Figure 4

Three-On-One MIM Configuration

in making good contact to the top field plate, even with a Ga-In
blob contact, lead to inconsistencies in the data. The majority of
the experiments were performed on samples of the first type.

    2. Substrate

        The MIM junctions were formed on circular glass sub-
strates one inch in diameter. The glass was ground, polished and
optically flat. Vapor from boiling trichloroethylene was used to
remove particles and grease adhering to the surface. A close inspection
under a 60x microscope was used to reject samples with obvious surface
imperfections. Grazing illumination made the detection of surface

scratches easier. The substrates were then cleaned again, immediately before being placed in the vacuum chamber.

3. Metal Electrodes

The upper and lower electrodes of the junction were formed by vapor deposition. In the large majority of cases Al, 99.99% pure, was used as the electrode material. The Al was vaporized by a five-turn tungsten heating coil located about 20 cm. from the substrate. Two sheet Al masks, each with a single slit 1.2 mm wide, were held within .5 mm of the substrate to form the electrodes. Because the masks could not be pressed directly against the substrate, the width of the Al electrodes varied from sample to sample. A 10x Zeiss calibrated eye-piece was used to determine the actual width of the electrodes and it was found that the junction area varied from 1.5 mm^2 to 1.75 mm^2. The experimental V-I characteristics were normalized to 1.4 mm^2 in each case to account for the varied junction area.

The electrodes were made sufficiently thick, about 700 – 1200 $\overset{o}{A}$, so that the junction current was controlled only by the properties of the thin insulating layer. A strip of the deposited Al, 2.5 cm. in length and 1.3 mm. wide had about 15 ohms dc resistance. Since the resistance is in series with the junction, on the order of 10^9 ohms, it is considered quite negligible.

Al was especially easy to vaporize and had good electrical properties. However, in the second of the above mentioned configurations, it proved especially hard to contact electrically, resisting even Ga-In as a contact wetting agent. Future experiments are planned with silver electrodes.

4. Polymer Insulator

The metal electrodes were separted by a thin insulating film of polymerized hydrocarbon as described by Ennos[13] and Christy[14,15,16]. This film was composed of interwoven strands of polymerized tetramethyletraphenylsiloxane, found in the vacuum system as D C 704 diffusion pump oil (Dow Corning Cehmical Co., Midland, Michigan). This oil was present in the system as a result of back-streaming from the diffusion pump and from an extra heated source located near the substrate. The polimerization activation energy was provided by a 350v electron beam, however the rate of film formation should not depend on electron energy since it has been observed[15] that only a few ev are necessary to cause one cross link to form. The number of cross links formed may be dependent on the electron energy only if the incident electrons are sufficiently energetic to penetrate a portion of the already formed film.

The rate of film formation is strongly dependent on the oil molecule arrival rate and the temperature of the substrate which governs how long an oil molecule will remain on the surface. If the electron/oil arrival rate ratio is high, every oil molecule hitting the surface will be polymerized, and the growth rate is sharply dependent on the conditions of the oil in the system. If the ratio is low, every incident electron will find one or more molecules and the growth rate will depend on the electron arrival rate. Electron current densities of $8\mu amps/cm^2$, $12\mu A/cm^2$ and $14\mu A/cm^2$ were used. Provisions for heating or cooling the substrate were not provided but it is felt that it remained quite close to room temperature throughout the polymerization process.

The polymer film was chosen as the insulating layer since it has several attractive properties.

a) The polymer film could be grown with reproducible characteristics and employed independent of the substrate material or the electrode metal. This is quite an important concept in that it makes available for study and comparison junctions of several different electrode materials.

b) It has been shown [15,16,17,18] that the film can be grown at a predictable, linear rate.

c) Because of the interwoven nature of the polymer it can be made quite uniformly thick and relatively free of pinholes. The immensity of the polymer molecules causes them to form in a preferred direction, presumably parallel to the surface of the substrate. For this reason the orientation of the tunneling current with respect to the polymer "quasi" lattice is always known.

d) The film is very durable as will be seen in Chapter III.

C. MIM Construction

1. Bell Jar System

The fabrication of the tunneling junctions was done in a glass bell jar pumped by a three stage NRC diffusion pump using D C 704 oil. The entire system was capable of vacua in the low 10^{-6} mm. of Hg range with overnight pumping, however, 3×10^{-5} mm was easily reached in an hour and the vapor deposition and polymer growing were done in this region.
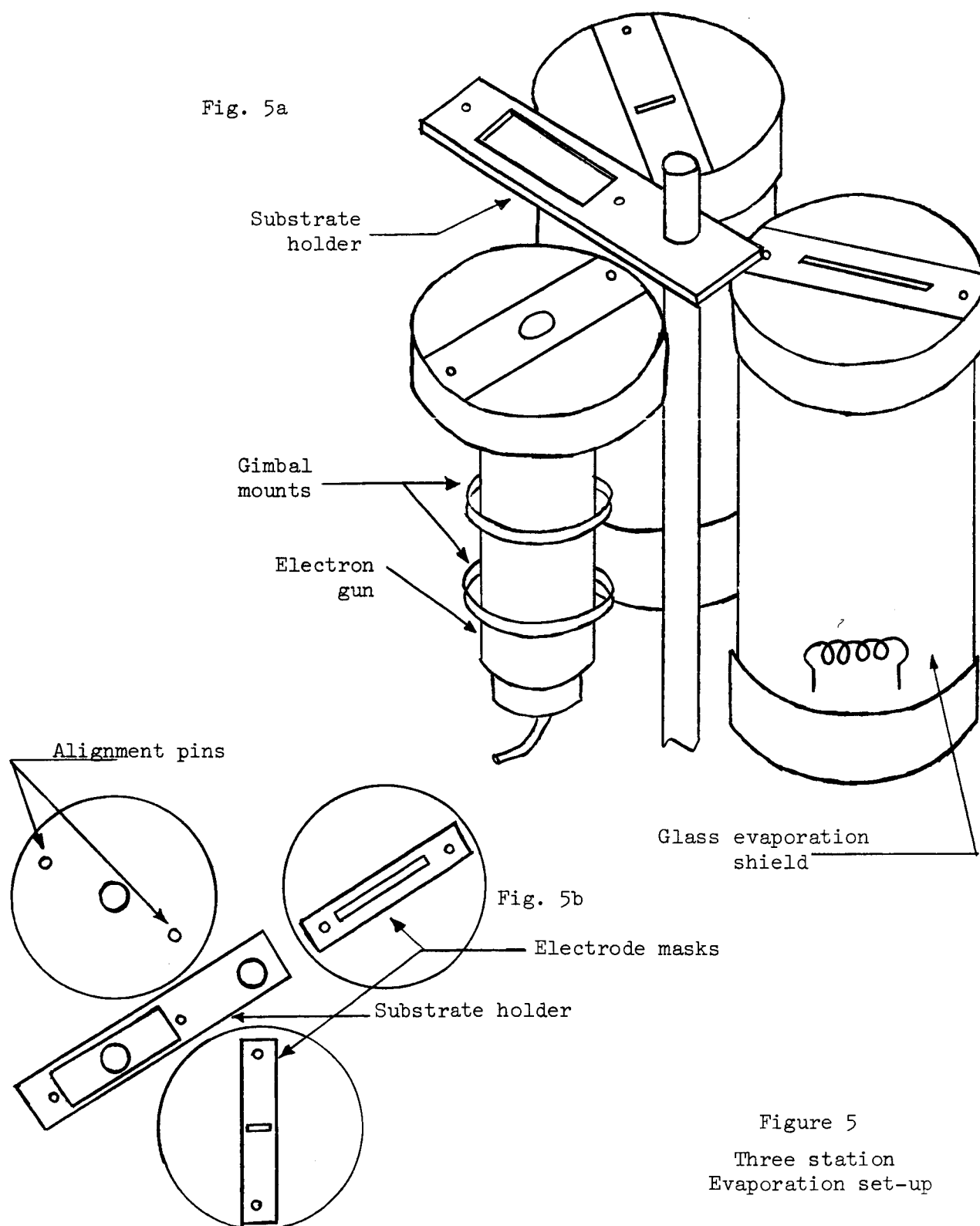
The bell jar was equipped with a three-station metal-polymer

deposition set-up, as described by Wilmsen[18], so that the entire process could be carried out without exposure to the atmosphere. This set-up consisted of two metal vapor deposition stations and a set of gimbaled rings to hold the electron beam source (see Fig. 5a). Each vapor deposition station was a glass cylinder 25 cm. high and 10 cm. in diameter with the tungsten filament at the bottom and the electrode mask at the top. With the sample in position over the mask, the filament was entirely enclosed, preventing any metal vapor from contaminating the rest of the system. The gimbaled rings held the electron gun in alignment with the target and were sufficiently sturdy to prevent misalignment during reloading procedures.

A pair of hand-operated controls, working through vacuum feed-throughs, rotated the sample holder from station to station and, in each position, lowered it onto a pair of alignment pins to assure accurate positioning. The procedure is described by a top view in figure 5b.

The sample holder could be moved from one position to the next rather quickly so that little contamination could adhere to the exposed metal-polymer interface between steps. The vacuum deposition shields were sufficiently long to keep the substrate, or the already-deposited polymer, away from the tungsten filament. This was thought to be especially important in the latter case to prevent asymmetries from occuring in the tunneling junction.

A small extra oil source was incorporated in the bell jar to increase the supply of oil molecules on the substrate available for polymerization. A small crucible of D C 704 (surface diameter-- 4 cm^2) was suspended in a tungsten filament about 40 cm. from the

Fig. 5a

Substrate
holder

Gimbal
mounts

Electron
gun

Glass evaporation
shield

Alignment pins

Fig. 5b

Electrode masks

Substrate holder

Figure 5

Three station
Evaporation set-up

polymerization site. The oil could be heated by means of the filament and the temperature monitored with a copper-constantan thermocouple. It was customary to allow the extra source to remain hot in the vacuum for at least an hour before each sample was made in an effort to reach equilibrium.

An attempt was made to keep the vacuum system free from contaminants, especially those of an organic nature as described by Ennos[13], however, it was impossible to assess to what extent the system was actually contaminated or what effect this contamination may have had on the experimental results. The entire system was cleaned periodically with trichloroethylene to remove accumulated oil, etc. The metal parts (almost entirely Al) in proximity to the substrate were stripped of surface contamination in a weak solution of NaOH. Except for loading and reloading, the system was kept sealed and evacuated at all times.

2. Electron Beam

The polymerization electrons are supplied by the electron gun from a 3BPI cathode ray tube. The face and the upper portion of the neck of the tube were removed and it was immediately transferred to the gimbal mount in the vacuum system. An external control circuit was used to provide for the aiming of the beam on the substrate, accelerating potential adjustment, beam current monitoring and adjustment and a focus control to vary the diameter of the polymer insulator. The control circuit is outlined in figure 6. The substrate was not biased above the final anode to collect secondary electrons since Christy[15] found that this increased the growth rate no more than 10%.
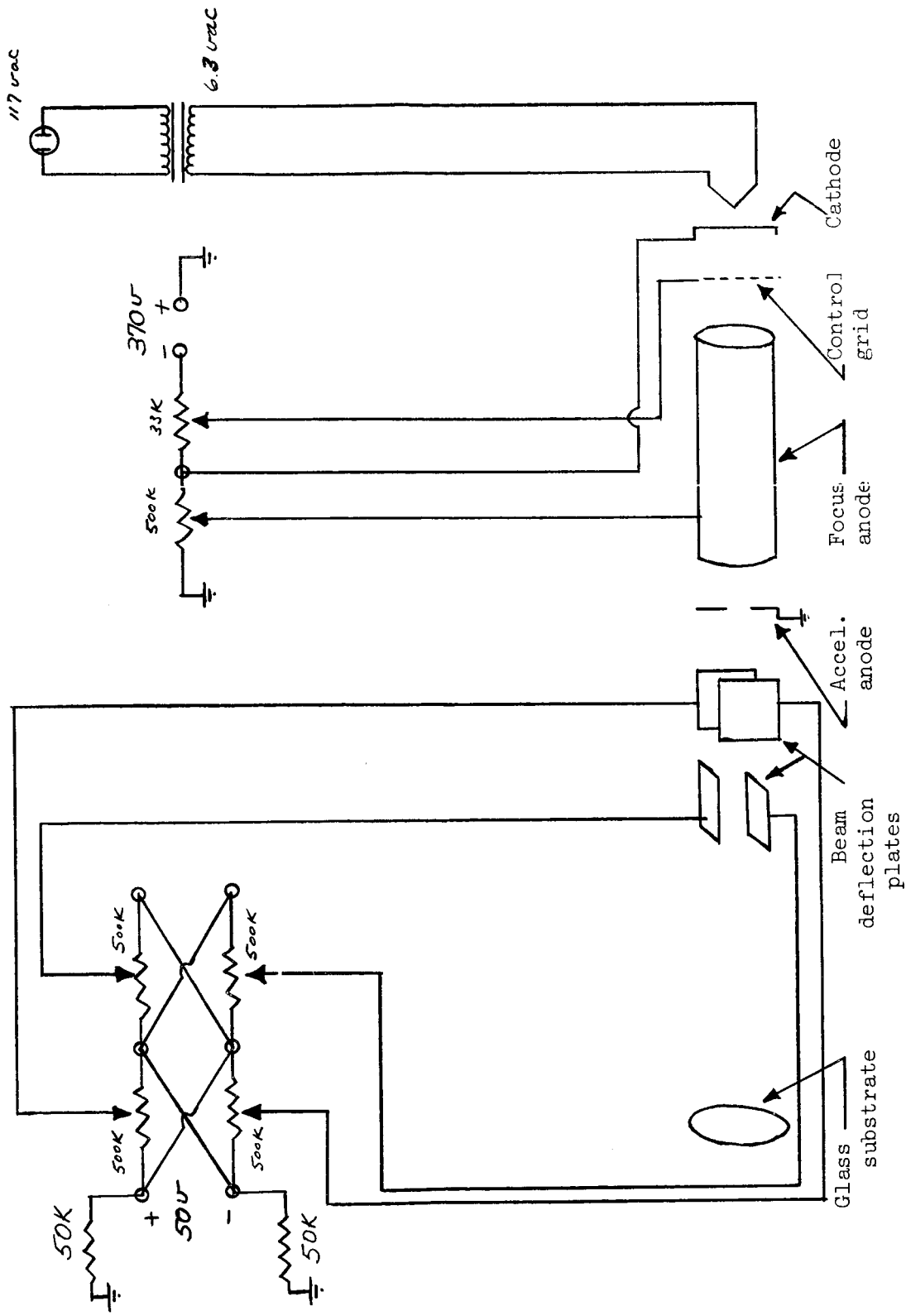
Figure 6

Electron Beam and Control Circuit

Exposure to the atmosphere would, at times, foul the surface of the cathode in the CRT. Since this would cause the electron beam to have some nonuniformities in its cross section, the cathode was cured by operating the filaments at 9 volts for about 10 minutes before each run.

D. Testing the Sample

1. Determination of Thickness

The primary thickness measurements of the polymer film were obtained by capacitance measurements. Using a parallel plate approximation and assuming a uniform thickness, the thickness of the junction may be written as

$$S = \frac{K\varepsilon_0 A}{C}$$

where K = relative dielectric constant

A = the area of the junction

C = the capacitance of the junction

The capacitance measurements were made on a General Radio type 1615A capacitance bridge at 1 kc. With the dissipation factor corrected for, a very sharp null could be had--sharp enough to resolve less than 10 pf. out of 6000 pf. The bridge had an overall error of not more than 0.5%. Capacitance derived from the sample holder and leads was always subtracted from the bridge reading. This extra capacitance was usually on the order of 3 pf.

The oscillator and detector in the bridge were tunable between 200 cps and 30 kc, allowing capacitance vs. frequency measurements to be made.

A second series of measurements made with a Gaertner Scientific

Ellipsometer provided not only an excellent independent check on the thickness measurements but provided information on the index of refraction, optical dielectric constant and film thickness uniformity. A computer program written by Yeargan[19], correlates ellipsometer angular readings with thickness for every 50 $\overset{o}{A}$. The program was written for an Al-on-glass substrate and all of the calculations were made for indices of refraction of 1.0, 1.1, 1.2 . . . 2.0. By interpolation of the program, thicknesses could be judged to be within 20 $\overset{o}{A}$ or less. Accuracy on the thicknesses of samples below 100 $\overset{o}{A}$ is somewhat questionable.

2. V-I Characteristics Bridge

The current through the junction for a given applied voltage was measured with a bridge that became unbalanced in proportion to the sample current. The advantage of the bridge is that currents of 10^{-12} amps may be measured without having to consider the input impedance of a series ammeter. Figure 7 shows the schematic of the bridge. The input impedance of the meters used, a pair of Hewlett-Packard H.P. 425's, is included in the analysis of the bridge and, when the sample is not in the circuit, the bridge is balanced with Vm_2 serving as one leg. When the sample is then replaced, the unbalanced voltage as read by Vm_1 is proportional to the sample current by the relation

$$I_s = 1.13 \times 10^{-5} \, V_4 \text{ amps}$$

The performance of the bridge was tested frequently with precision 1% resistors from 10 meg. to 10k. The bridge was always within the 1% tolerance. Noise was kept at a minimum by shielding all components and using a pair of coax cables from the bridge to the sample.
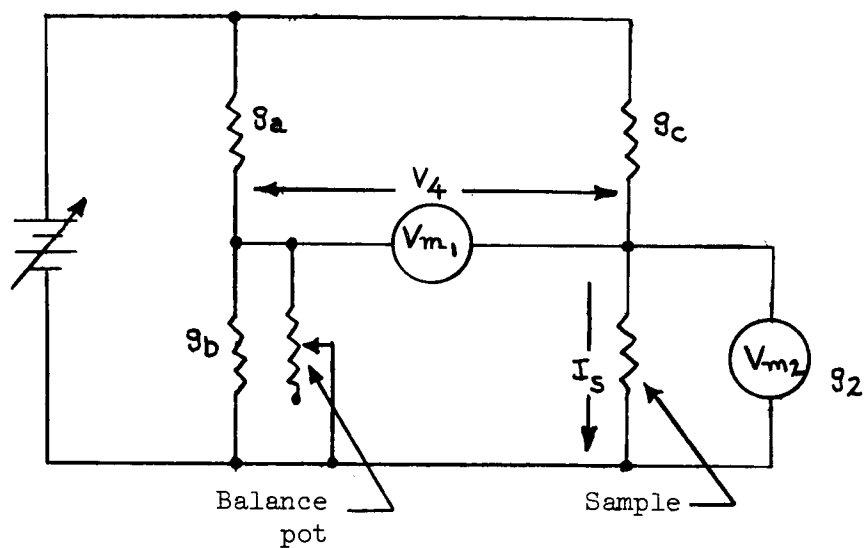
$$I_s = \left(\frac{g_c g_e + g_1 g_a}{g_a} \right) V_4$$

where

$$g_e = g_a + g_b + g_1$$
$$g_1 = \text{input impedance of } V_{ml}$$

Figure 7

V-I Characteristics Bridge

CHAPTER III

EXPERIMENTAL RESULTS

A. Introduction

Over a period of three months, fifty MIM tunneling junctions
were constructed and tested in various ways. The construction tech-
nique, described above, was kept as uniform as possible over the en-
tire group of devices. Data was analyzed after each group of two or
three samples was built and tested in order to make future experiments
more fruitful. A serious problem with device yield was encountered
and several subtle steps had to be adopted in the construction pro-
cedures. In actuality, roughly two fifths of the devices fabricated
yielded good data. The other portion suffered from outright short
circuits through the polymer, thin spots in the insulator which broke
down under the mildest stress,or characteristics that were too eratic
to yield meaningful data whatever the cause.

The data obtained may be broken into two categories: the
electrical characteristics of the sample operated as a non linear
device and information about the nature of the dielectric itself or
the other materials or processes involved in the current transport.

B. Voltage-Current Characteristics

1. V-I Curves for Varying Thicknesses

Figure 8 shows the characteristic curves for six rep-
resentative thicknesses. V-I characteristics were taken for all of
the samples that were not outright shorts and, in general, all fell
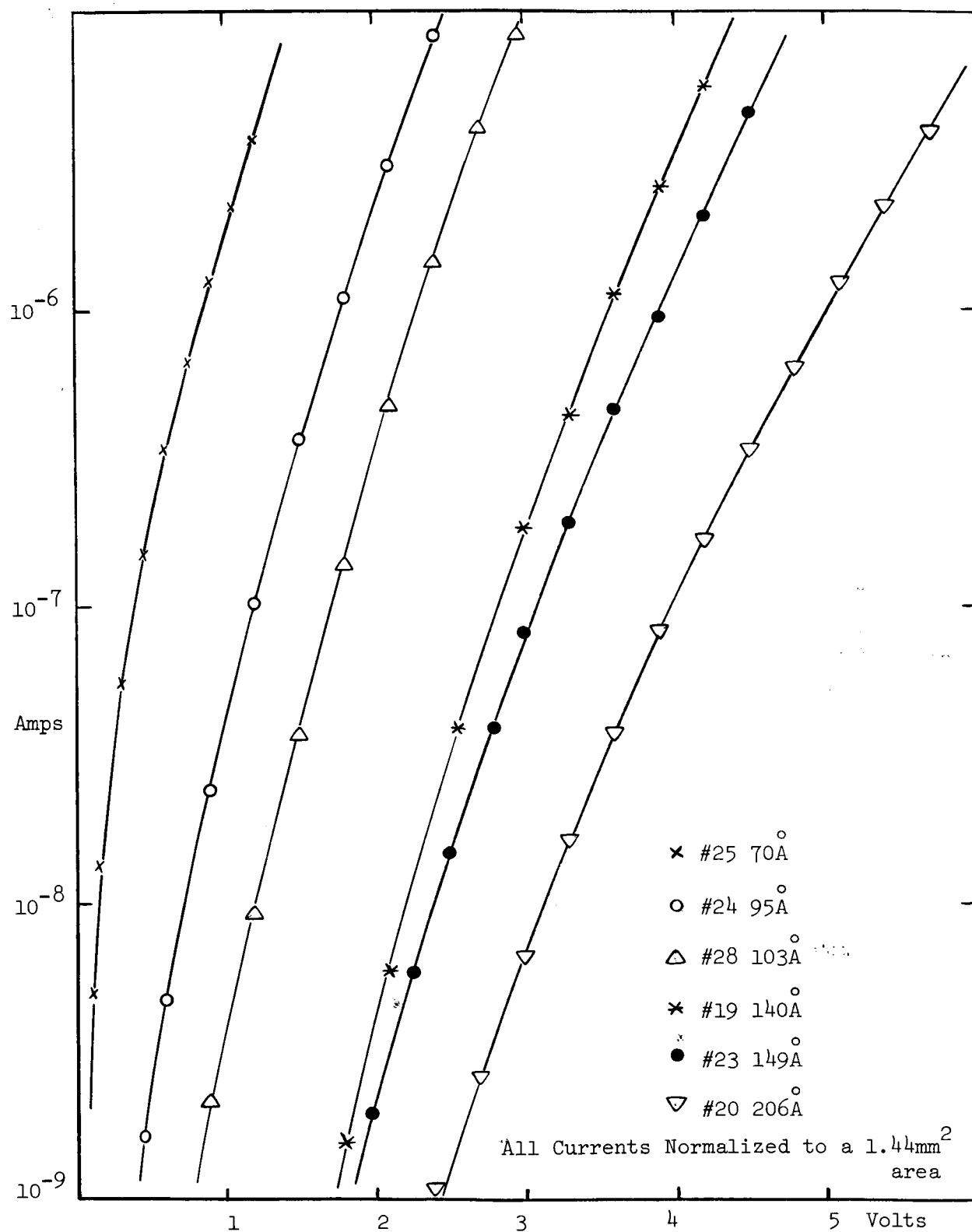in the family of curves in figure 8. Almost every sample that deviated

Figure 8

V-I Characteristics as a Function of Thickness

seriously from this pattern could be found to have a defect that accounted for the lack of conformity with the others. The curves shown were all made with the bottom electrode, i.e. the electrode contiguous to the glass, at negative polarity. The tests were made in the open air immediately after the sample was removed from the vacuum and usually required no more than 10 to 15 minutes to complete. Before the devices were removed from the vacuum they were allowed to remain for 10 minutes in order to allow the Al electrodes and the polymer to order itself and to reach a stable configuration.

The characteristics are quite similar to those of Wilmsen[18]. They differ in that these are translated slightly to the right of his, i.e. for a given thickness about 15% more voltage was required to reach the same current density. Also, the slopes of his curves are slightly greater than the ones in figure 8.

The characteristics in figure 8 are plotted $\ln I$ vs V^1 to facilitate comparison with Stratton's equation. The data points did not form a straight line when graphed $\ln I$ vs $V^{1/2}$, nor was a straight line observed on log-log paper. This last plot was important since Rose[20] predicts that, if the current is space charge limited it will be proportional to V^n.

The highest current densities recorded were generally on the order of 10^{-3} amp/cm^2. Although most of the samples did not break down at this point, they were stressed to the point where current readings became quite unstable. The breakdown field for several samples biased until shorting occured was found to be about 5×10^6 v/cm. Christy[15] and Mann[17] report the breakdown of similar films at 10^7 v/cm.

2. Hysteresis

The V-I characteristics of the MIM junction are rather dependent on the immediate past history of the electric field in the insualtor. If the current at a given voltage is measured, the bias increased and then returned to the original value, the current increase is as much as 100%. This effect can be seen in figure 9. The current returns to its original value in time, hence the data in figure 9 is only qualitative since no time rate of change of voltage or current is defined.

A forming or polarization effect was also observed. If the field was held constant at some moderate level, the current slowly decreased to some intermediate value over the period of several minutes. However, if the field was completely removed, relaxation to zero bias state was quite rapid. These observations correspond quite closely to those made by Mann[7] on polymer films between 500 and 2500 $\overset{o}{A}$. Penley[21], working with $Al-Al_2O_3-Al$ junctions finds similar evidence for polarization charge formation. He notes that when a constant field was held across the device the current slowly decreased; upon reversing the polarity for a few minutes and then going back to the origianl direction, the current quickly rose to its initial value and then began to decrease again.

3. Polarity

Very little rectification was observed in the junctions tested if the sample was allowed to relax for several minutes between stressings at opposite polarities. This seems to indicate that the insulating barrier is quite symmetrical and that both of the interfaces between the electrodes and the insulator are relatively uniform. If
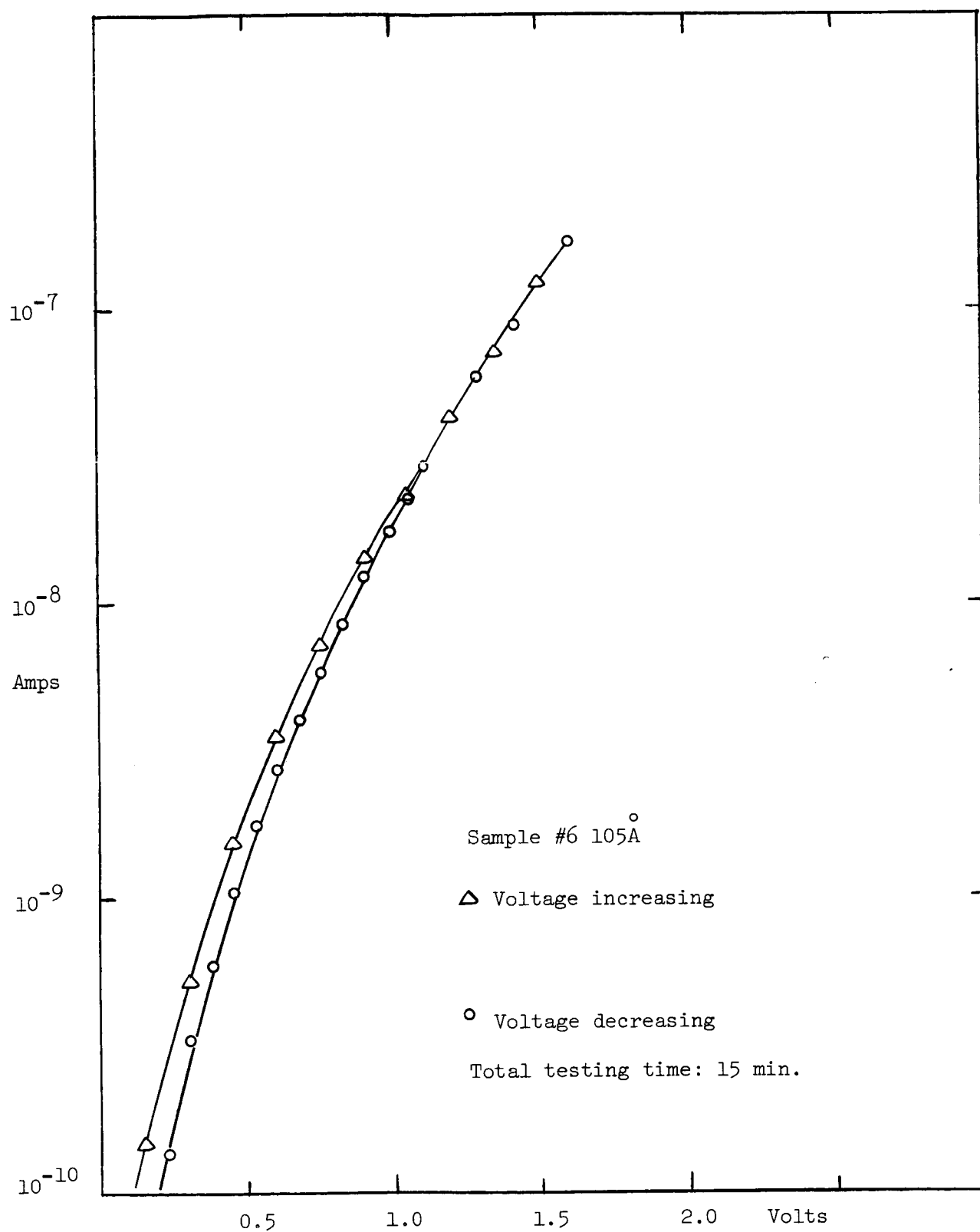
Figure 9

Hysteresis at Low Fields

the sample was not given time in the unstressed state but was tested
at the opposite polarity immediately, the current at a given voltage
was always higher than at the same voltage of opposite polarity.
This seems to indicate that the polarization field set up to oppose the
initial field increases the effective field in the insulator when the
opposite bias is applied.

4. Stratton's Equation

Stratton's equation (25) may be written in the form

$$I = \frac{AI_o}{2} \exp(-b_{11}V^2) \exp(\frac{C_{10}}{2} V) \tag{30}$$

for moderate voltages. The equation is not valid as V approaches
zero nor is it accurate for voltage much larger than ϕ_o, the bar-
rier height. This latter restriction is due to the nature of the coef-
ficients b_{11} and C_{10} as terms in an infinite series expansion. As
the voltage becomes higher, more terms in the expansion must be retain-
ed to extend the validity of equation (30) into that region.

Due to the approximate nature of these coefficients, equa-
tion (30) reaches a maximum current at $V = \frac{C_{10}}{4b_{11}}$ and then begins to
decrease. Obviously, since this has no foundation in experimental
reality, $V = \frac{C_{10}}{4b_{11}}$ is a maximum upper bound of the voltage range for
equation (30) as it stands.

Simmons' equations (16, 17 and 18) are valid over the range
of voltages from zero to much larger than ϕ_o. However, the equations
are in such a form to make them untractable for comparison with experi-
mental data. Unterkofler[22], with the use of a computer, derives curves
from Simmons' equation for various thicknesses, barrier heights and

Sample #24, 95 $\overset{\circ}{A}$

O Experimental Data

△ Points Calculated from Stratton's equation using

$\dfrac{C_{10}}{2} = 7.3$

$b_{11} = 1.1$

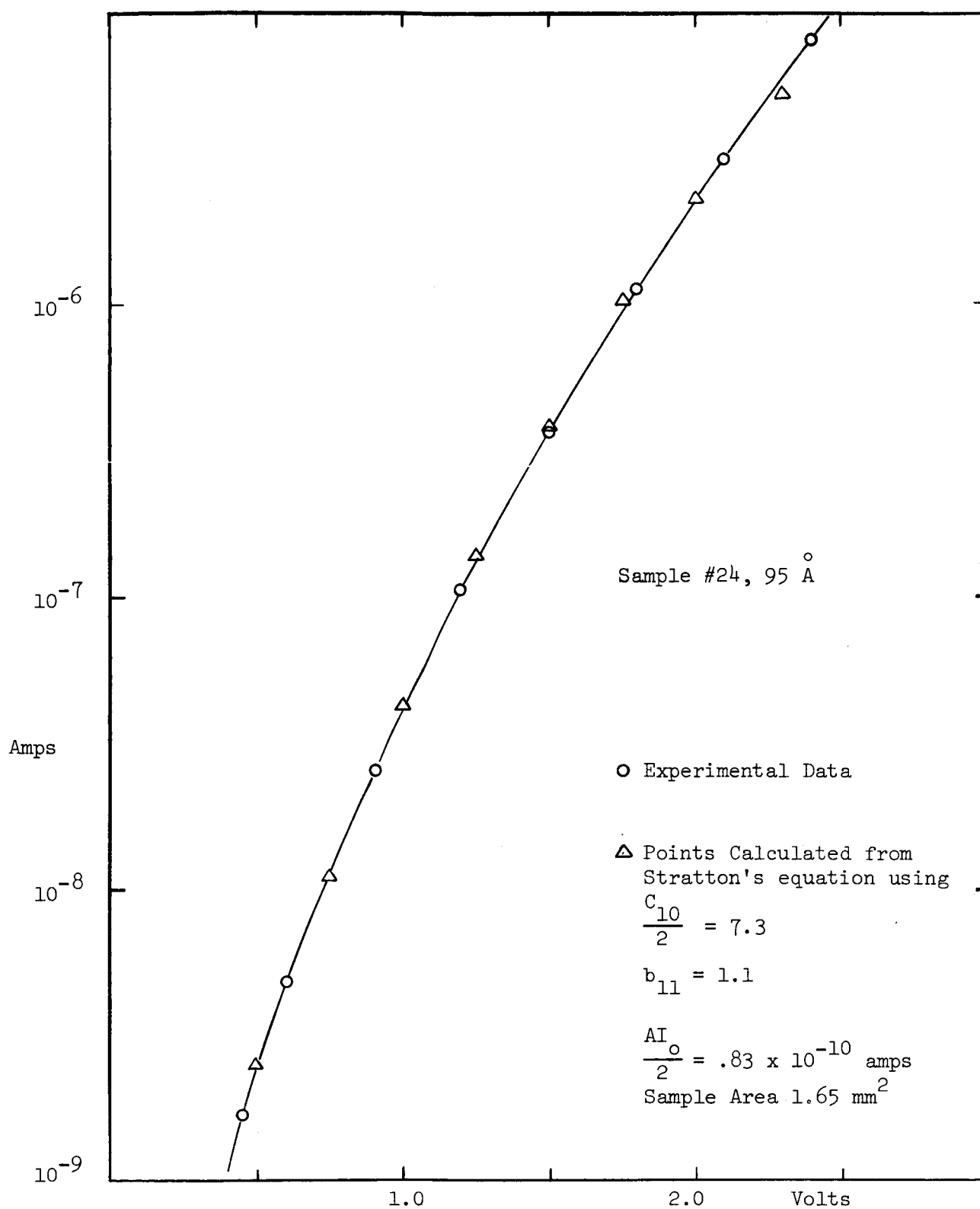$\dfrac{AI_o}{2} = .83 \times 10^{-10}$ amps

Sample Area 1.65 mm^2

Figure 10

Stratton's Equation Fitted to Experimental Data

dielectric constants. Unfortunately, he limits his discussion to thick-
nesses under 50 $\overset{o}{A}$ and only trends for thicker devices could be seen.

Because of its relative simplicity, Stratton's equation was
chosen for comparison with the experimental data. Figure 10 shows the
experimental data for sample number 25 (95 $\overset{o}{A}$) and Stratton's equation(30)
with the parameters $C_{10} = 14.6$, $b_{11} = 1.1$ and $\frac{AI_o}{2} = .83$ x 10^{-10} amps.
The agreement is quite good up to 2 volts; after this point the theo-
retical equation begins to loose validity. The parameters chosen are
quite close to those used by Stratton[10] and Wilmsen[18] for slightly
thinner films.

5. V-I Characteristics of Thicker Samples

Five samples were constructed with thicknesses ranging
from 400 to 800 $\overset{o}{A}$, thicknesses ususally thought of as the domain of
thermal or Schottky emission. It was hoped that, since tunneling
had been observed and identified in films over 100 $\overset{o}{A}$, samples could be
constructed at progressively greater thicknesses and the gentle transi-
tion from one mechanism to another could be observed.

Figure 11 shows two of the curves for samples 540 $\overset{o}{A}$ and 770 $\overset{o}{A}$
Only two curves are shown, however similar characteristics were ob-
tained for all five samples. A sharp change in slopes was observed
in all cases. The horizontal axis of figure 11 is in $(volts)^{1/2}$
since Schottky emission in the form of equation (29) was expected.
Equation (29) predicts the slope ,g,of a curve that is true thermal
emission, when plotted ℓnI vs $V^{1/2}$, should be given by

$$g = \frac{1}{kT} \left(\frac{e^3}{4\pi K\epsilon_o}\right)^{1/2} \frac{1}{s^{1/2}}$$

10⁻⁸

#31 540Å 1.2 mm²

#32 770Å 1.2 mm²

10⁻⁹

A
m
p
s

10⁻¹⁰

10⁻¹¹

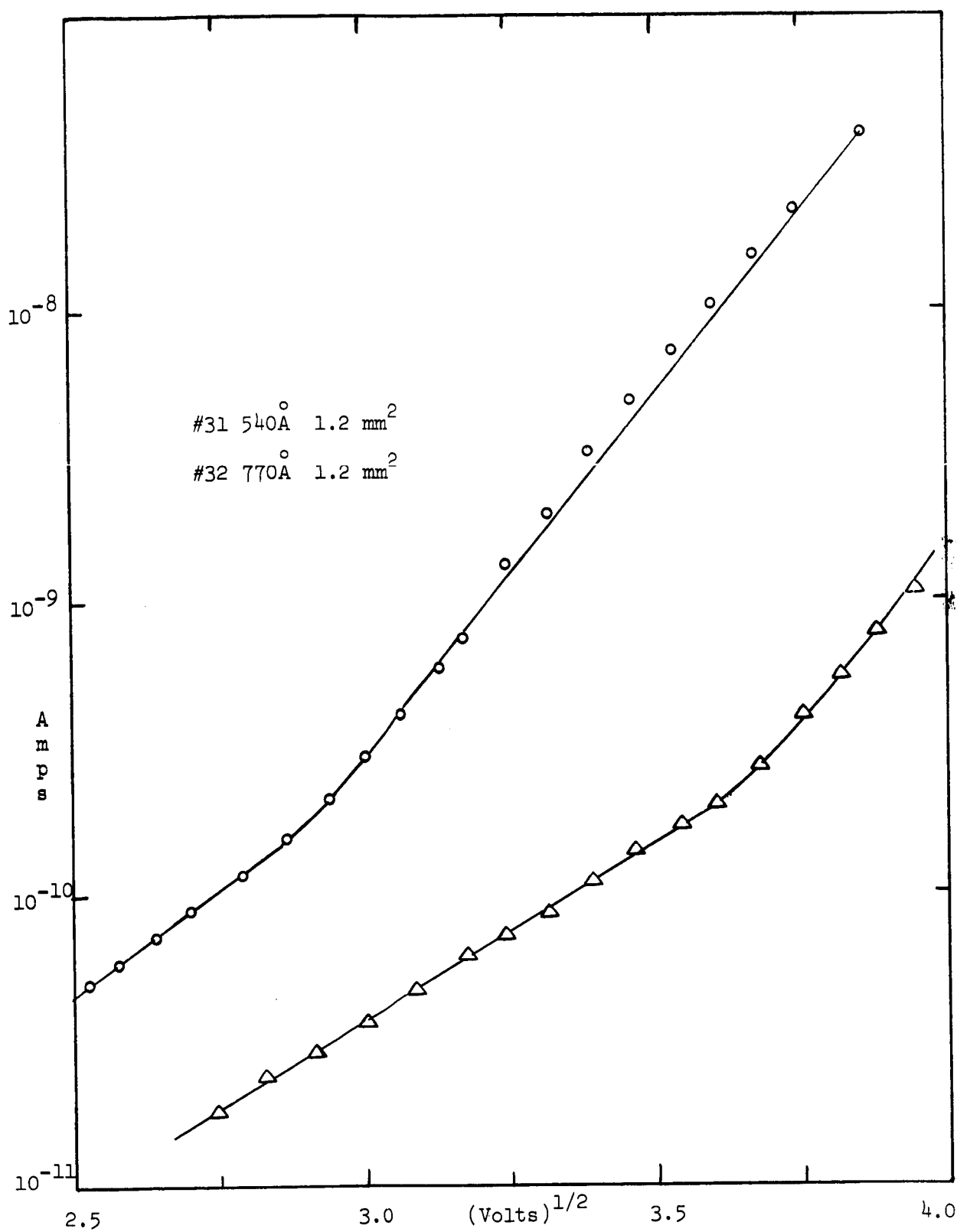2.5   3.0   (Volts)^{1/2}   3.5   4.0

Figure 11

V-I Characteristics of Thick Junctions

where K = relative dielectric constant

s = insulator thickness

If we assume K = 2.8 (see Ch. III, D 2) and that T = $297°K$, the theoretical slopes for a thermal emission mechanism for s = 540 $\overset{o}{A}$ and 770 $\overset{o}{A}$ are

$$g_{540 \overset{o}{A}} = 3.8 \ (volt)^{-1/2}$$

calculated

$$g_{770 \overset{o}{A}} = 3.15 \ (volt)^{-1/2}$$

The measurements of the slopes of the lower portions of both curves in figure 11 yield

$$g_{540 \overset{o}{A}} = 3.85 \ (volt)^{-1/2}$$

slope measured
below break

$$g_{770 \overset{o}{A}} = 3.09 \ (volt)^{-1/2}$$

It appears, then, that the data below the break is primarily due to thermal emission.

If the data is then plotted on a Fowler-Nordheim scale ($\ln \frac{I}{V^2}$ vs $\frac{1}{V}$) as in figures 12 and 13, it is seen that the portion of the curve above the break is asymptotic to a straight line. However, if the thermal contribution of the current is subtracted (by extrapolating the lower portion of the curve in figure 11) from the total, the remainder falls on a straight line. Because of this and other arguments presented in the following section (effective mass etc.) it is thought that the upper portion of the curves represents the onset of field emission as the predominant mechanism.

Most studies on tunneling quoted above, both theoretical and experimental, have concentrated on tunneling through insulators with
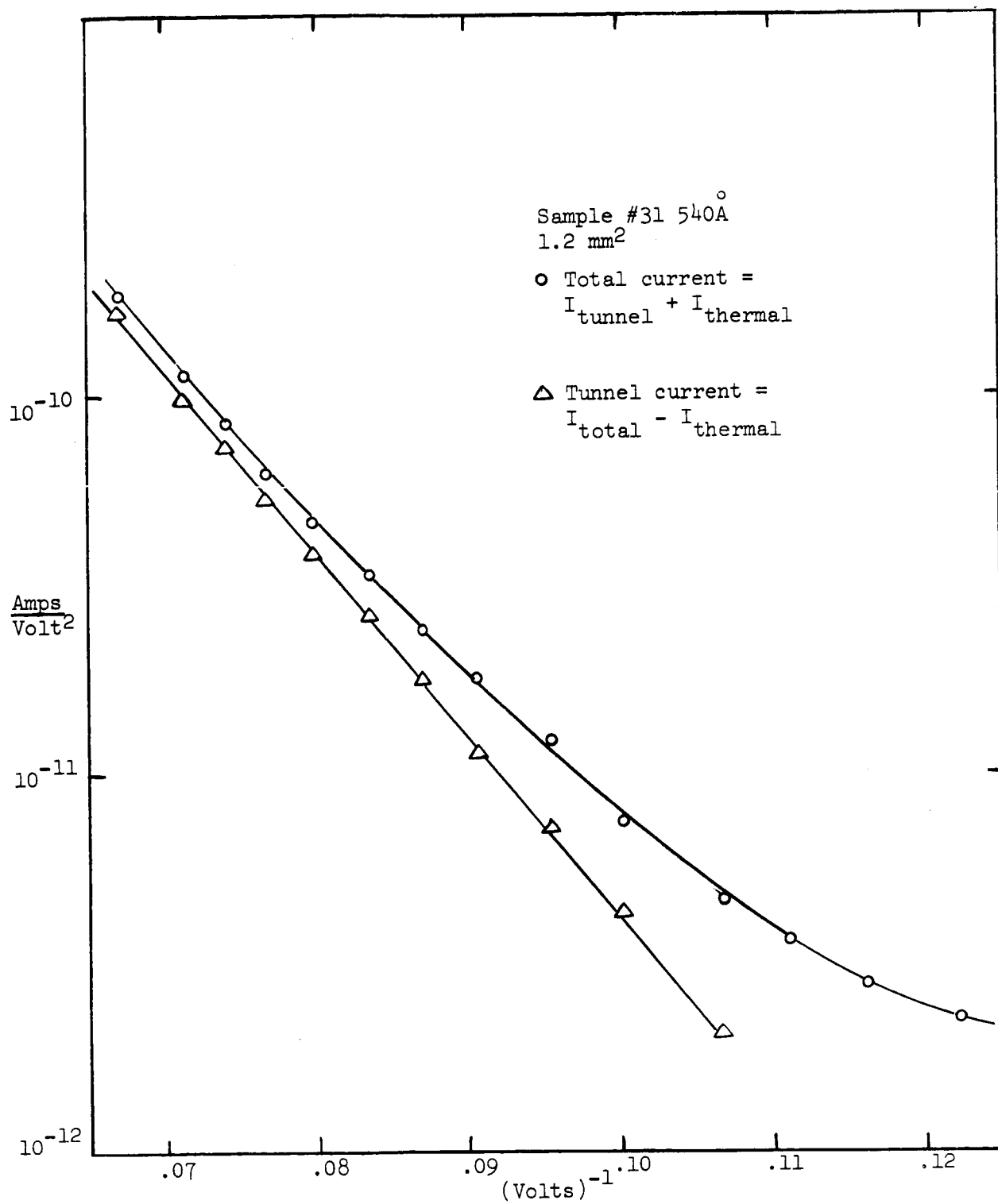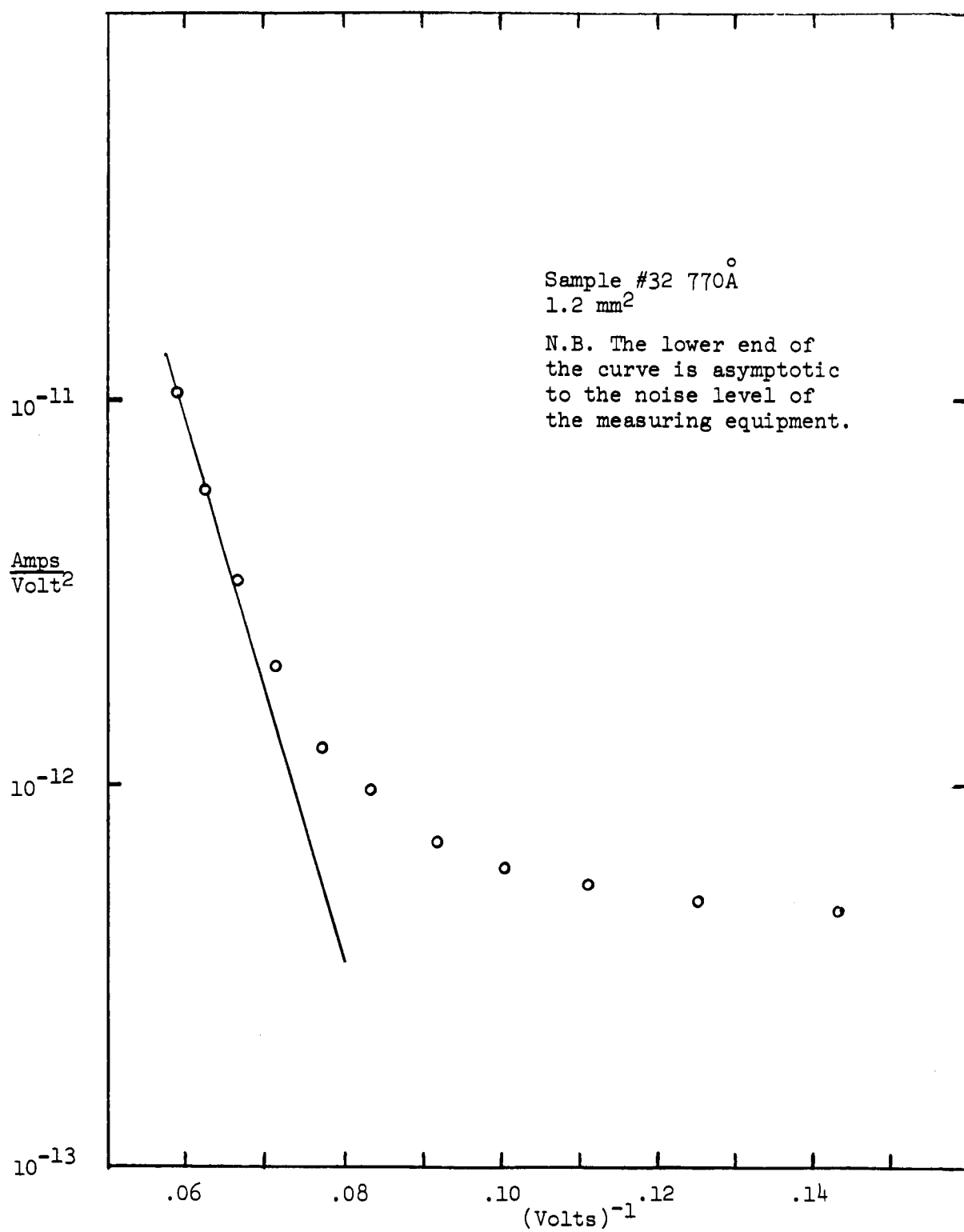
Figure 12

Fowler-Nordheim Plot, Sample # 31

Sample #32 770Å
1.2 mm²

N.B. The lower end of
the curve is asymptotic
to the noise level of
the measuring equipment.

Figure 13

Fowler-Nordheim Plot, Sample #32

thicknesses of 50Å or less. This, however, does not indicate that the
phenomina does not occur in thicker films. Simmons[5] hasfound that the
barrier height and effective tunneling thickness are both functions of
applied voltage (equations 12, 13 Chapt. I). Using these relationships,
the effective thickness of a 540Å insulator with an unbiased barrier
height of 1.09eV and with 11 volts bias applied is 50.6Å. The effective
height of the barrier under the same conditions is .397eV. Using the
above values and equation(18b), the current density is calculated to
be 9.5×10^{-8} amps/cm^2. Consulting figure 11, it is seen that the tun-
neling current at this point is 1.1×10^{-7} amps/cm^2. The discrepancy in
the current values is small and easily overcome by changing the barrier
height only slightly. Hence, it seems quite probable that both mechanisms
have been observed in operation simultaneously and correctly identified.

C. Barrier Parameters

1. Barrier Height

The Schottky thermal emission equation is explicit in
the barrier height ϕ_o where ϕ_o is measured from the Fermi level of the
adjacent electrode at zero bias. When V= 0, the thermal current from
equation (29) is

$$J(V=0) = 120T^2 \frac{m^*}{m_e} \exp(-\phi_o/kT)$$

where T = temperature in °K.

    m^* = the effective mass of the electron in the conduction band
        of the insulator.

    J = thermal current in amps/cm^2.

From figure 11, the zero bias intercept for sample 31 is

2.5×10^{-14} amps/cm^2. Therefore, for T = 297^{0}K

$$\phi_o = \frac{1}{38.8} [(2.3)(18) - \ell n(\frac{m}{m*})(.695)]$$

If we assume that m*/m = 1 then ϕ_o = 1.08ev

For m*/m = 0.1 then ϕ_o = 1.02ev

Similar calculations made with sample 32 result in

ϕ_o = 1.1ev when m* = 1

ϕ_o = 1.04ev when m*/m = 0.1

Experience with carriers in the conduction band of semiconductors and semimetals makes it reasonable to assume that m*/m is less than 0.5. On this basis $\phi_o \simeq$ 1.05 ev.

2. Effective Mass

In the preceeding section a guess was made about the effective mass of the electron in the conduction band of the polymer. The effective mass of the electron in the forbidden band of the insulator may be calculated from the tunneling data, however. When V>>ϕ_o/e, the tunneling current given by the equations of Simmons or Stratton reduces to an expression quite similar to the Sommerfield-Bethe equation. This expression is

$$J = \frac{2.2e^3V^2}{8\pi h\phi_o s^2} \ exp \ [- \frac{8\pi s}{2.96heV} (2m)^{1/2} \phi_o^{3/2}] \qquad (31)$$

The factors 2.2 and 2.96 arise due to the depression of the barrier by the external bias. The argument of this tunneling equation is explicit in ϕ_o. The slope, b, of a J/V^2 vs. 1/V plot may be written

$$-b = \frac{-8\pi s}{2.96he} (2m^*)^{1/2} \phi_o^{3/2}$$

The slope b, for sample 31 from figure 12, is 1.37×10^2 volts. In order that the experimental slope be identical with that calculated from theory

$$\frac{m^*}{m_e} = 0.114$$

For sample 32, figure 13, the slope is 1.82×10^2 volts. In this case $\frac{m^*}{m_e} = 0.105$.

Stratton[10] calculates the coefficients of his series expansions in terms of the parameters of the system [equation (24)]. In this way, he writes

$$C_{10} = \frac{2\pi s (2m^*)^{1/2}}{h \phi_o}$$

For sample 24

$$C_{10} = 14.6$$
$$s = 95 \overset{o}{A}$$

In this case $\frac{m^*}{m_e} = 0.105$

These calculations seem to be in fair agreement with those made by others. Christy[16], working with an identical polymer insulators finds $\frac{m^*}{m} = 0.13$. Fisher and Giaver[23], experimenting with thin films of Al_2O_3 report effective masses of 0.11.

D. Other Experimental Results

1. Polymer Growth Rate

Christy[15], Mann[17] and Wilmsen[18] report that the thickness of the polymer insulator was a linear function of time. Figure 14
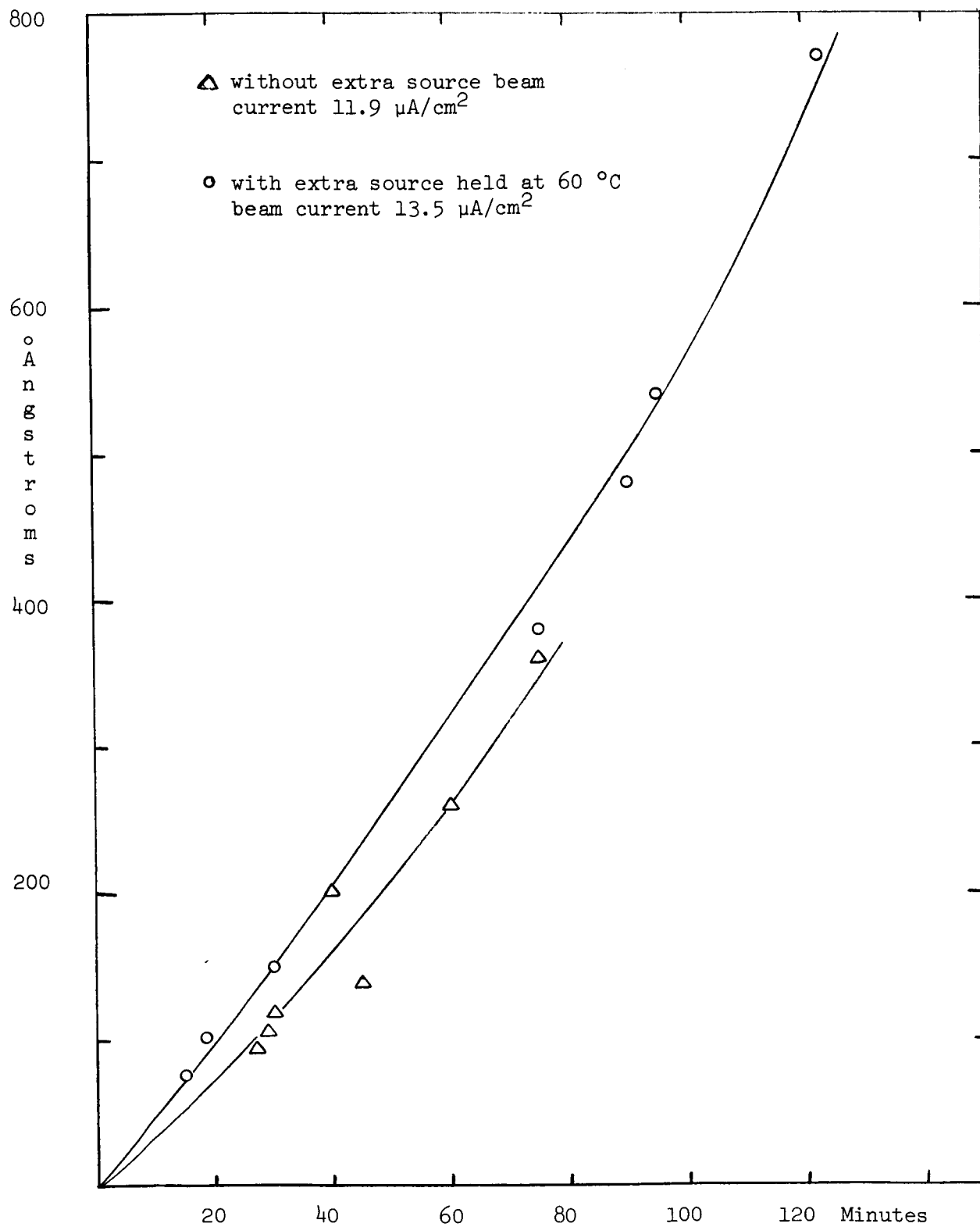
Figure 14

Polymer Growth

shows that this was not the case, especially for the samples with the extra source and higher beam current. During the experiments, it was noted that, with the extra source, the growth rate was highly dependent on the time the extra source was given to come into equilibrium with the bell jar atmosphere. Most times the extra source was heated to and kept at 60°C. for one hour before the polymer was formed. It seems quite possible that the system had not approached equilibrium in this time but that the number of oil molecules in the vacuum continued to increase during the growth period resulting in what appears to be an acceleration in the growth rate.

It can be seen from the curve, that the D C 704 allowed to enter the system from the diffusion pump played an important role in the growth rate. At one point, when the oil charge in the pump had been altered chemically by oxidation, the growth rate became very small.

2. Dielectric Constant

Since capacity measurements were used to determine the thickness of the films, it was important that the dielectric constant be known with some degree of accuracy. Christy[15] and Ennos[18] found the relative dielectric constant to be 2.8. Thicknesses calculated from capacity measurements using K = 2.8 are correlated with those taken by an interferometric technique using an ellipsometer in figure 15. The agreement seems to be quite good.

The data from the ellipsometer also indicated that the index of refraction of the polymer is 1.5 and that the optical dielectric constant is 2.25. Christy[15] stated that, from purely visual methods, he judged the index of refraction to be between 1.6 and 1.8. Because of the precision of the ellipsometer and the extensive program used
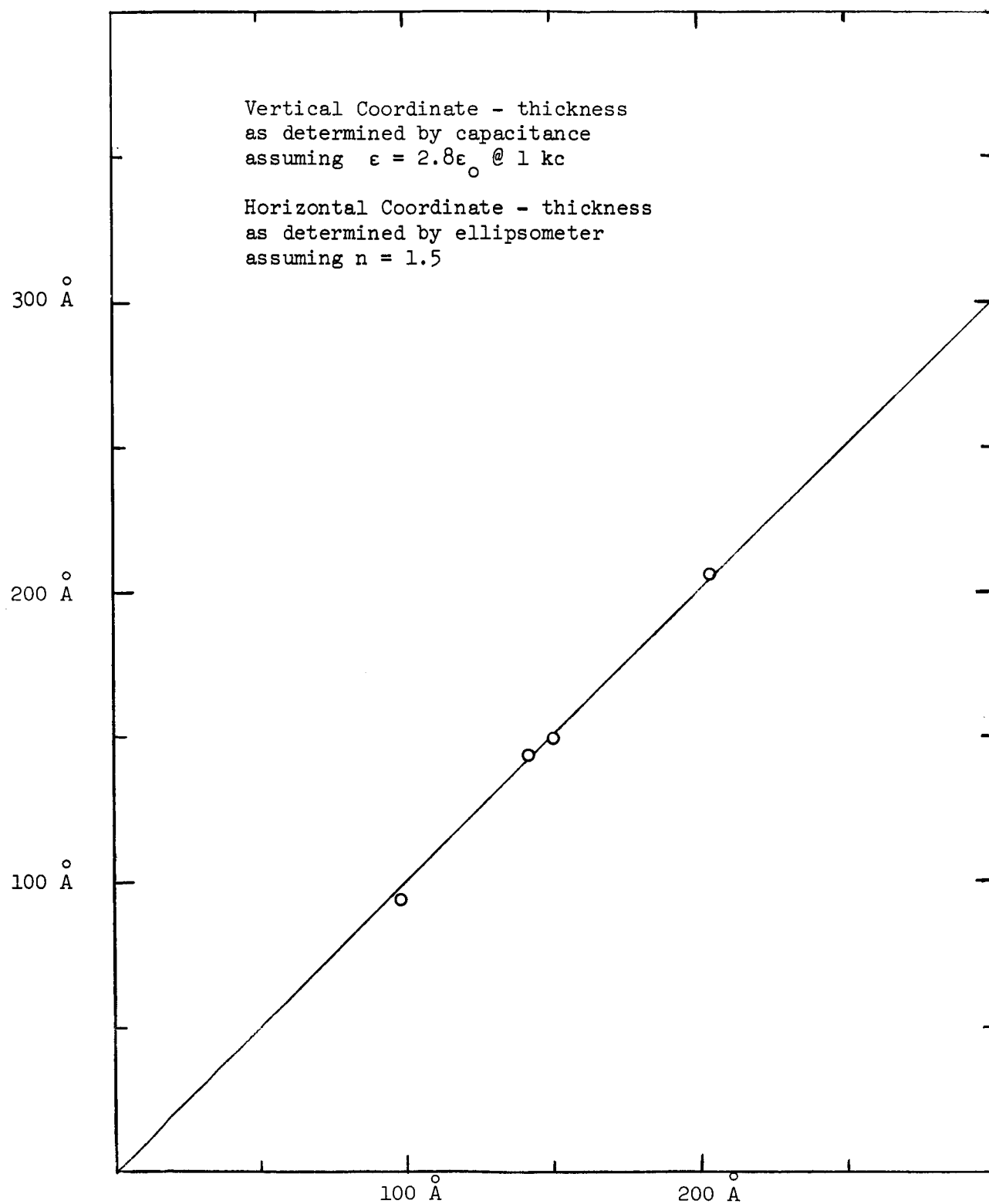
Figure 15

Determination of Dielectric Constant

to analyze the data, it seems quite probable that the index of refraction is close to 1.5.

Figure 16 shows the frequency dependence of the capacitance for a 70 Å sample. Such dependence at low frequencies is completely unexpected in common dielectrics and may indicate a Debye-Frohlich[33] relaxation mechanism with an associated activation energy at work in the polymer. Because of the complexity of the molecules, numerous relaxation processes may be present. The massiveness of the molecules suggests a low frequency associated with the mechanism. Analysis of loss tangent versus frequency data for NaCl and KCl by Grissom and Hartwig[34] leads to specific conclusions about the nature of the relaxation mechanisms and their specific causes in these alkali halides. Because of the amorphous nature of the polymer, similar conclusions may be more difficult to reach.

3. Temperature Dependence

The temperature dependence of the tunneling phenomenon was observed by taking the tunneling junction from room temperature to that of liquid nitrogen and back to room temperature. The sample was placed in a helium atmosphere in the inner dewar of a double dewar system. The outer dewar was filled with liquid nitrogen and the temperature was allowed to drop while the current at a constant voltage and the temperatures were monitored continuously. The entire process took almost six hours to complete. To insure that any current change during this time was not due to the formation of a polarization change, the sample was allowed to "form" at the test voltage for over an hour before the test and the data was taken from room temperature to that of LN_2 and back to the starting point. Very little hysteresis was
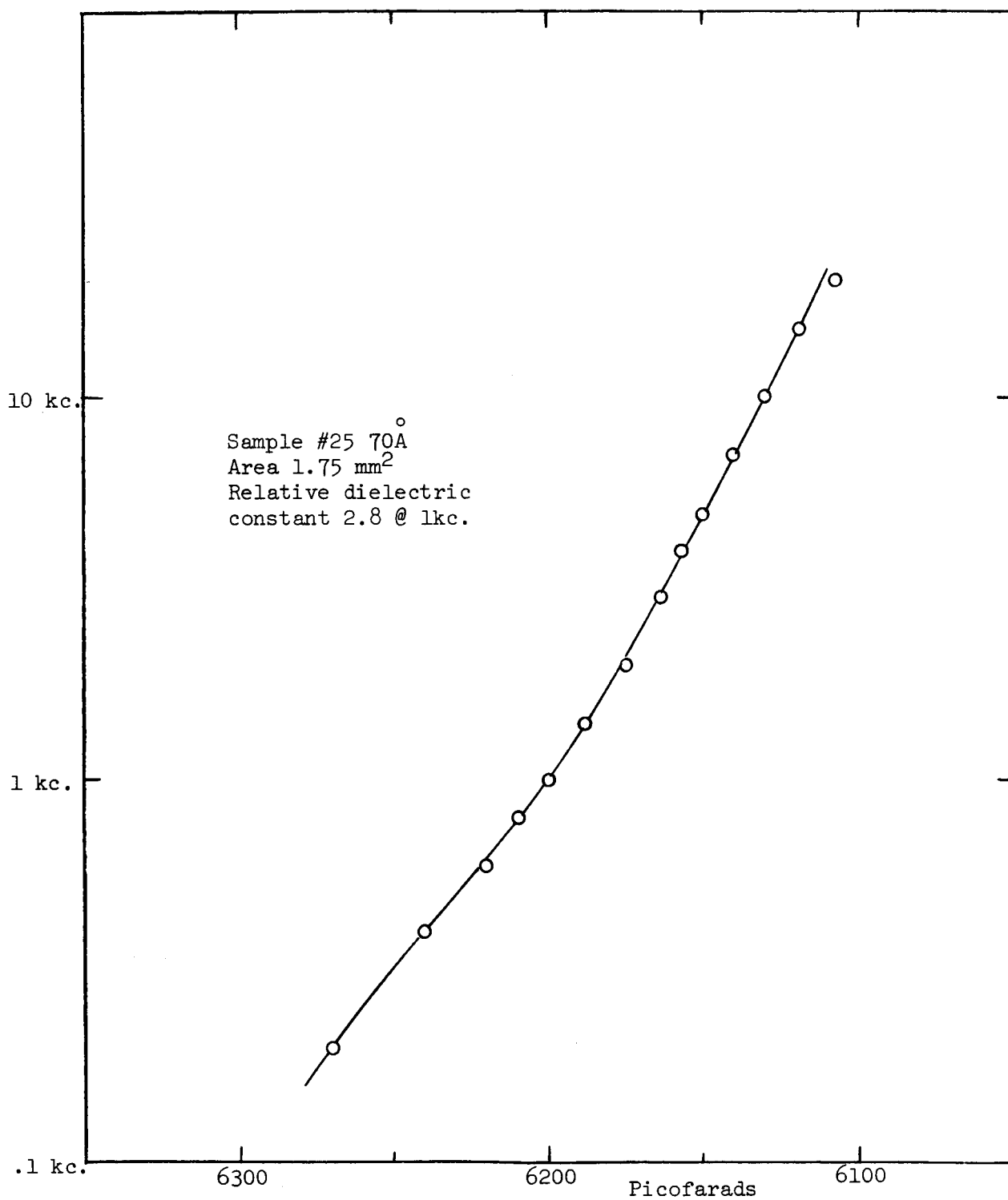
Figure 16

Capacitance vs. Frequency

observed.

No data was taken by heating the sample since the onset of thermal emission may have made the data useless.

The data is plotted in figure 17. The T^2 dependence is quite good. I(0) was obtained by extrapolating the experimental points to $T = 0^{\circ}K$ on a linear scale. The total change in current from $T = 297^{\circ}K$ to $T = 80^{\circ}K$ was roughly 20%. This agrees quite well with the experimental results achieved by Hartman and Chivian[24] and the theoretical calculations made by Simmons[9].

4. Aging

The electrical properties of the junctions were observed to vary rather markedly with time. Because of this fact, a large number of tests could not be made with any one sample. Tests that were made, were completed as quickly as possible so as to approximate roughly uniform electrical properties throughout the experiment. In general, a sample stored in air for any length of time showed a translation to the right (with respect to the previous V-I characteristics) i.e. more voltage was required to maintain the same current through the junction. The slope of the curves were also reduced somewhat, i.e. the current was slower to increase with voltage. The aging characteristics varied somewhat from sample to sample tested, however figure 18 a,b shows results which are quite typical. Sample 25 (70 $\overset{o}{A}$) was kept in a vacuum since fabrication. The first 42 hours showed some translation of the characteristics to the right. However, during this time an increase in the capacitance was also noticed, indicating possibly that the polymer film was increasing in thickness. Such an increase would result in the translation to the right (see figure 8). At t = 49 hours,
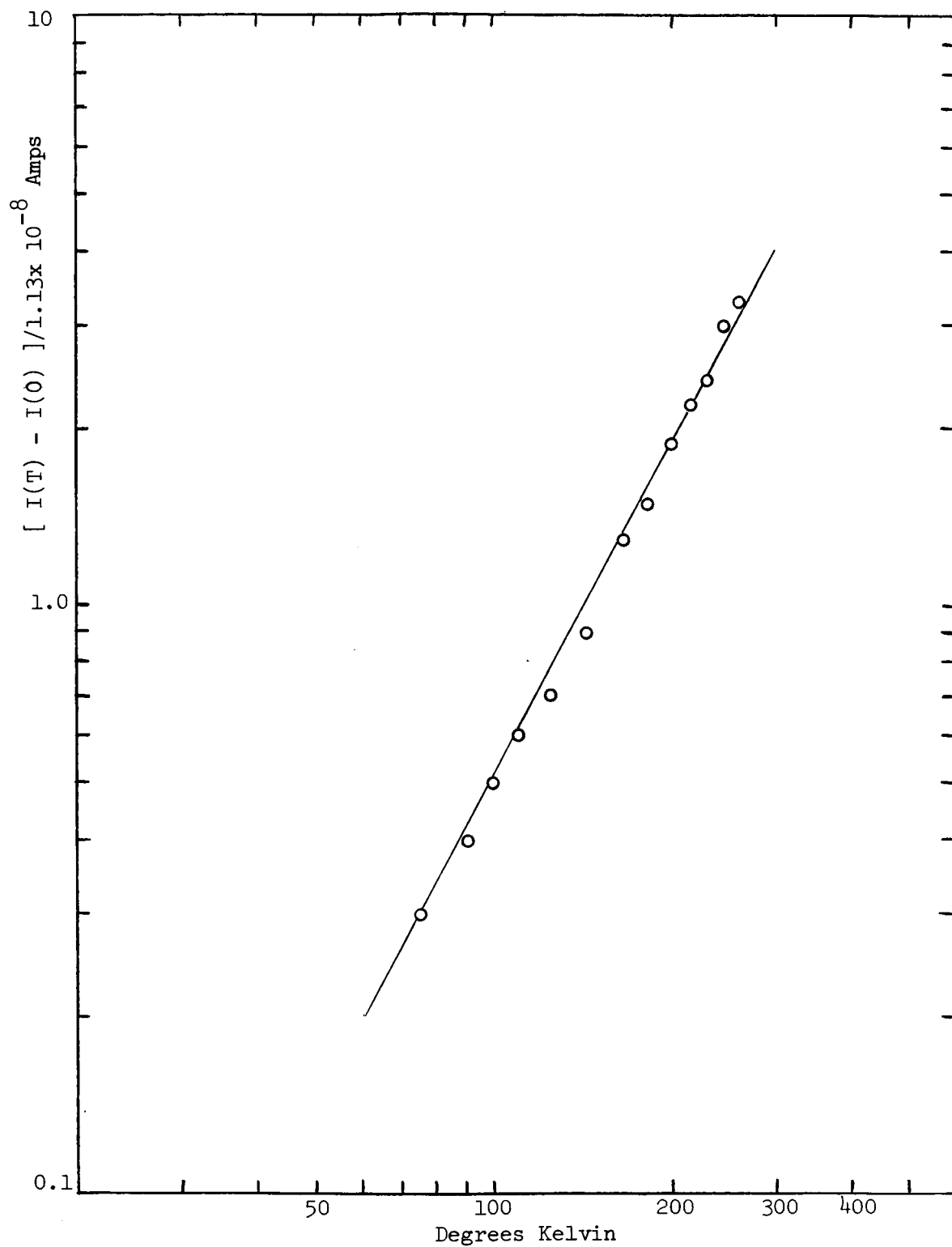
Figure 17

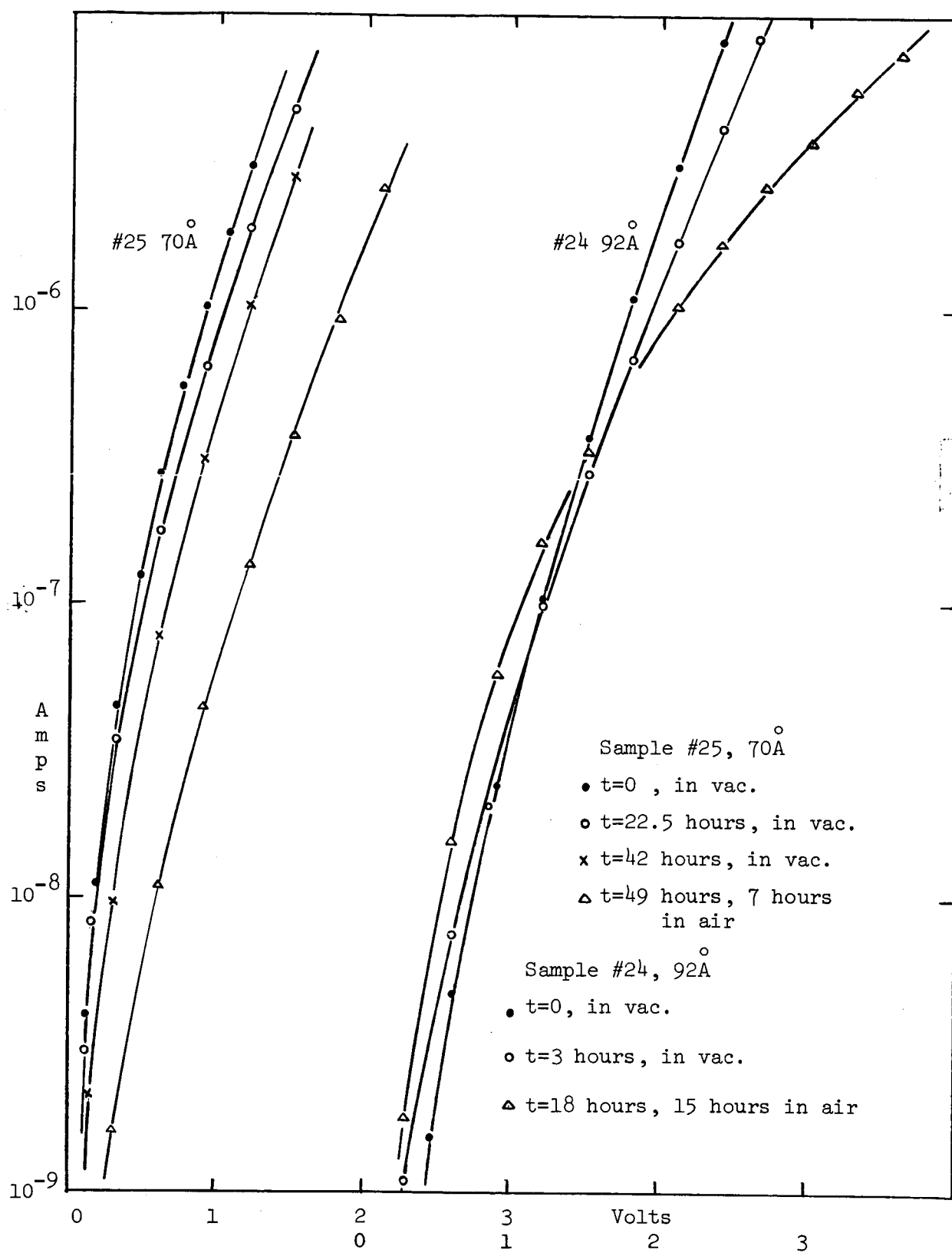Temperature Dependence of the Tunneling Phenomenon

Figure 18

V-I Characteristics as a Function of Time

the sample had been exposed to the atmosphere for 7 hours. Little

change in capacity was noticed yet the V-I characteristics changed

rather radically.

     Sample 24 (92 $\overset{o}{A}$) showed the same behavior as 25 while in the

vacuum but, once removed, the curvature changed somewhat drastically.

It is interesting to compare this curve after aging with that of sam-

ple 14, made immediately after removal from the vacuum. This is done

in figure 19. The insulator in sample 14 was made with a lower elec-

tron-to-oil ratio than that in sample 24. This gives support to Christy's[15]

argument that tunneling through a polymer film is a trap-aided process,

i.e. electrons caught in traps located physically inside the insulator

need tunnel only a fraction of the thickness to reach the anode.

These traps could be provided by free hydrogen radicals in the poly-

mer. The higher the electron-to-oil ratio at the time of polymeriza-

tion, the higher the number of free radicals. Hence, aging in a poly-

mer may be the result of chemical recombination of free radicals re-

sulting in fewer traps and more difficult tunneling. The diffusion

of contaminants from the atmosphere into the polymer would hasten the

process greatly. This effect would be especially noticeable at high

current densities where the limited numbers of traps from which tunnel-

ing could take place would have the effect of limiting the current.

     Mann[17] views the polymer aging process in a different light.

He reports no change in characteristics for samples kept under vacuum

conditions nor for samples kept in a dry atmosphere. He concludes

that aging is due to the absorption of H_2O vapor by the junction which

changes the dielectric constant. Hardy[25], working with Al_2O_3 insula-

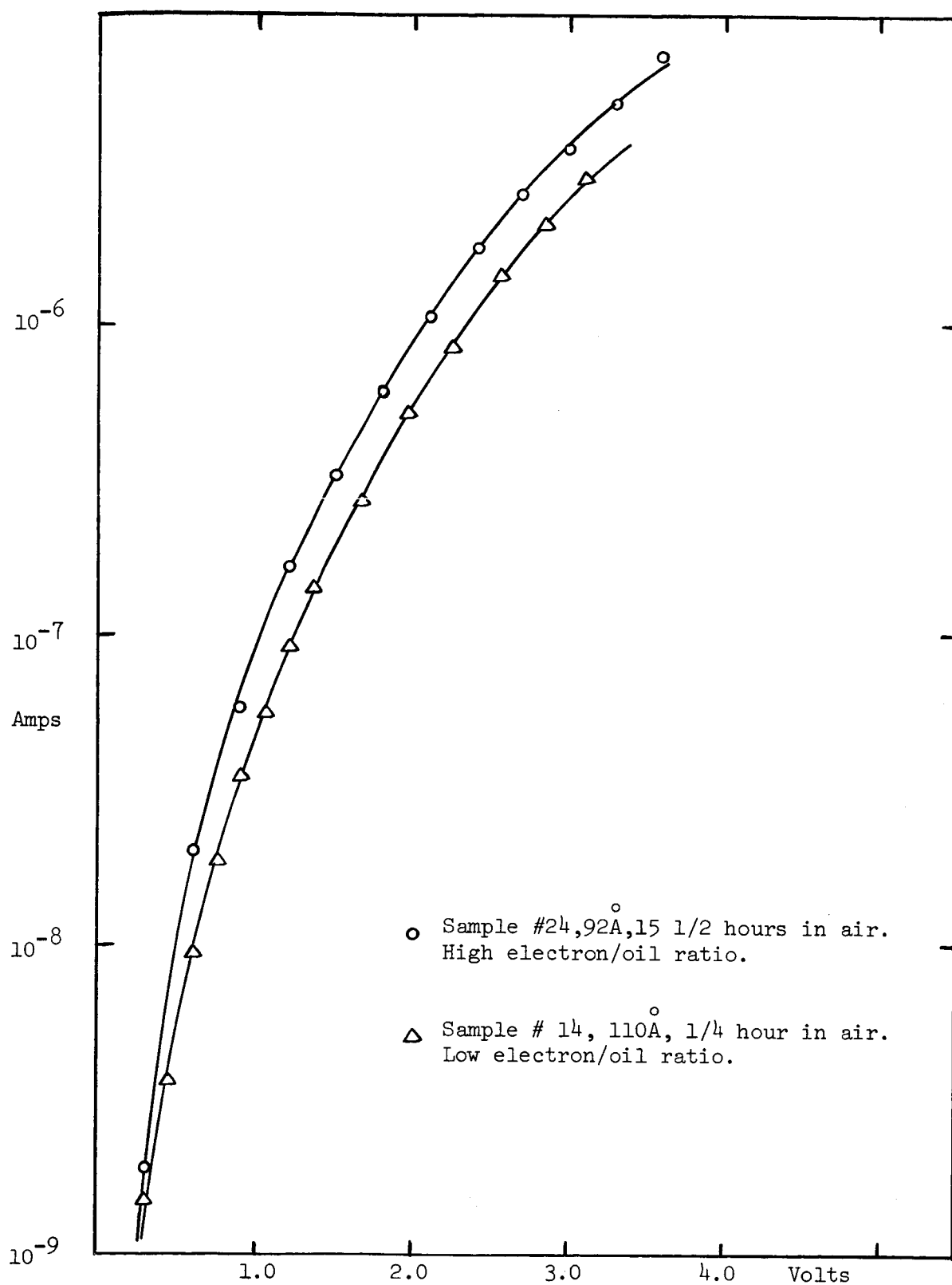tors believes the aging process to be the diffusion of electrode ions

Figure 19

Correlation of Electron /Oil Ratio with Aging

into the film. The size of the electrode atoms appears to be the factor controlling the penetration of the metal ions into the oxide and hence the junction resistivity. Theoretical equations for the altered barrier height and shape due to the diffusion of electrode ions into the metal are derived by Geppert[26,27]. Penley[21] observed a junction resistivity increase in proportion to the $\ln$ of time. He theorizes that this change is due to the diffusion of Al_2O_3 into the metal electrodes making the dielectric appear wider and the resistance of the junction higher.

Hartman and Chivian[24] overcoated an Al-Al_2O_3-Al junction with a thick layer of SiO sealing it off from the atmosphere. A small amount of aging did occur thereafter, but is was slight in comparison with junctions left open to the atmosphere. After aging for 4 months, the resistance change was about .1% in 3000 min. When the device was then tested "no shorting, hysteresis, long time constant, forming, negative dynamic resistance or change in the direction of rectification was observed."

5. Failure Mechanisms

Because of the rather low device yield, the mechanisms causing the failures were studied and steps were taken to avoid them in the future. The majority of failures were outright short circuits or became ohmic as soon as voltage was applied. These samples were systematically destroyed in order to discover the nature of the failures. Because the polymer was chemically inert in the presence of all chemicals tried (H_2SO_4, HCl, HNO_4, NaOH, NH_4OH, acetone, benzene, xylene, pentane, boiling trichlorethylene, etc). a method of selective etching was used. A drop of moderately strong NaOH was placed

on the junction. The top electrode was attacked and carried away. However the bottom electrode was touched only where the polymer was missing i.e. had an extremely thin spot or pin hole. The bottom electrode was then illuminated from the back and viewed under a 50K microscope. The holes let the light through and the trouble spot was usually readily obvious. The overwhelming majority of pin holes were caused by peaks or pock marks on the glass substrate. These peaks were usually small enough to go undetected in the preliminary examination. No real estimate could be made as to the height of the peak that caused catastrophic breakdown.

Erratic behavior was generally traceable to scratches in the substrate or plateaus on the surface. The scratches, often far too subtle to be seen in the initial inspection, became more apparent after deposition of the bottom Al electrode due to its high degree of reflectivity. The scratches seemed to result from improper grinding and polishing. Plateaus on the surface seemed to be the result of residue left on the surface by cleaning solvents. Chow[28] treats the problem of film non-uniformity and its effects on the tunneling characteristics, however his results were not applicable to such drastic cases as the above.

CHAPTER IV

SUMMARY OF CONCLUSIONS

Several conclusions may be drawn from the above research
about the MIM tunneling junction as a device and about the several com-
ponents in it. In rather abbreviated form, these conclusions are

(1) The V-I curves for the devices can be explained on the
basis of tunneling theory as expressed in the equations of Stratton[10]
or Simmons[5].

(2) The devices show some hysteresis at low voltages and
a characteristic forming time. This is probably attributable to the
formation of a polarization charge in or at the boundary of the in-
sulator.

(3) Aging of the sample may be due to the reduction in the
number of free radicals in the polymer. This reduction takes place
at an accelerated rate when the device is exposed to the atmosphere.

(4) Field and thermal emission occur simultaneously in the
thin film junctions. The two mechanisms can be separated and identi-
fied.

(5) The polymer insulator has a dielectric constant at 1 kc
of 2.8 and an index of refraction of 1.5. It presents a barrier height,
with zero bias applied, of about 1.05 ev. The effective mass of an
electron in the forbidden band of the insulator, travelling perpen-
dicular to the planes of polymer molecules, is 0.11 m_e.

(6) Successful tunneling junctions must be constructed on
substrates free of surface anomolies. Careful inspection under a micro-
scope of more than 50x is necessary to guarantee that this is so.

APPENDIX I

Stratton's equation fitted to sample 24A

$$J_T = \frac{AI_o}{2} e^{-b_{11}V^2} e^{\frac{C_{10}}{2}V}$$

$$b_{11} = 1.1 \qquad \frac{C_{10}}{2} = 7.3 \qquad \frac{AI_o}{2} = .83 \times 10^{-10} \text{ amps.}$$

V	$\frac{C_{10}}{2}V$	V^2	$b_{11}V^2$	$\left(\frac{C_{10}}{2}V - b_{11}V^2\right)$	$e^{(\ )}$	J_T
.5	3.65	.25	.27	3.38	29.37	2.45×10^{-9}
.75	5.48	.562	.617	4.86	129.0	1.07×10^{-8}
.9	6.56	.81	.89	5.67	291.	2.42×10^{-8}
1.0	7.3	1.0	1.1	6.2	492	4.08×10^{-8}
1.25	9.12	1.56	1.72	7.4	1636	1.36×10^{-7}
1.50	10.95	2.25	2.47	8.48	4850	3.95×10^{-7}
1.75	12.79	3.06	3.37	9.42	12300	1.02×10^{-6}
2.00	14.6	4.00	4.4	10.2	27000	2.24×10^{-6}
2.3	16.8	5.29	5.8	11.0	59600	4.95×10^{-6}

BIBLIOGRAPHY

1. Leighton, R. B. _Principles of Modern Physics_, p. 148, McGraw-Hill, New York, 1959.

2. A Messiah, _Quantum Physics_, p. 231 North Holland Publishing Co., New York, 1961.

3. N. F. Mott and I. N. Sneddon, _Wave Mechanics and Its Applications_, p. 15, Clarendon Press, Oxford, 1948.

4. Wang, S., _Solid State Electronics_, p. 370 McGraw-Hill, New York, 1966.

5. Simmons, J. G., "Generalized Formula for the Electric Tunnel Effect Between Similar Electrodes Separated by a Thin Insulating Film." _Journal Applied Physics_ 34, 1793 (1963).

6. Fowler, R. H. and Nordheim, L., "Electron in Intense Electric Fields," Proc. Roy. Soc. A119, 173 (1928).

7. Holm, R., "The Electric Tunnel Effect Across Thin Insulator Films in Contacts," _Journal Applied Physics_ 22, 569, (1951).

8. Simmons, J. G., "Electric Tunnel Effect Between Dissimilar Electrodes Separated by a Thin Insulating Film," _Journal Applied Physics_ 34, 2581 (1963).

9. Simmons, J. G., "Generalized Thermal I-V Characteristic for the Electric Tunnel Effect," _Journal Applied Physics_ 35, 2655 (1964).

10. Stratton, R., "Volt Current Characteristics for Tunneling Through Insulating Films," _Journal Phys. Chem. Solids_ 23, 1177 (1962).

11. Murphy, E. L. and Good, R. H., "Thermionic Emission, Field Emission, and the Transition Region," _Phys. Rev._ 102, 1464 (1956).

12. Johnson, D., _Field Effect Transistors,_ Chapter 3 Ed. by J. T. Wallmark and H. Johnson, Prentice-Hall, Englewood Cliffs, N. J., 1966.

13. Ennos, A. E., "The Sources of Electron Induced Contamination in Kinetic Vacuum Systems," _Brit. J. Appl. Phys._ 5, 27 (1954).

14. Christy, R. W., "Conducting Thin Films Formed by Electron Bombardment of Substrate," _J. Appl. Phys._ 33, 1884 (1962).

15. Christy, R. W., "Formation of Thin Polymer Films by Electron Bombardment," _J. Appl. Phys._ 31, 1680 (1960).

16. Christy, R. W., "Electrical Properties of Thin Polymer Films, Part II, Thickness 50-150Å." _J. Appl. Phys._ 35, 2179, July, 1964.

17. Mann, H. T., "Electrical Properties of Thin Polymer Films, Part I. Thickness 500-2500 Å," J. Appl. Phys. 35, 2173, July 1964.

18. Wilmsen, C. W., "Tunneling Between a Metal and Silicon Separated by a Polymer Insulator," Doctoral Dissertation, University of Texas, January, 1967.

19. Yeargan, J. R., "Current Mechanisms in Silicon Nitride," To be published.

20. Rose, A., Cocnepts in Photoconductivity and Allied Problems, p. 69 Interscience Publishers, New York, 1963.

21. Penley, J., "Aging of $Al-Al_2O_3-Al$ Thin Film Sandwiches," J. Appl. Phys. 33, 1901 (1962).

22. Unterkofler, G. J., "Theoretical Curves of Tunnel Resistivity vs. Voltage," J. Appl. Phys. 34, 3143 (1963).

23. Fisher, J. C. and I. Giaever, "Tunneling Through Thin Insulating Layers," J. Appl. Phys. 32, 172, Feb. 1961.

24. Hartman, T. E. and J. S. Chivian, "Electron Tunneling Through Thin Aluminum Oxide Films," Phys. Rev. 134, A1094 (1964).

25. Handy, R. M., "Electrode Effects on Aluminum Oxide Tunnel Junctions," Phys. Rev. 126, 1968, June 1962.

26. Geppert, D. V., "Theoretical Shape of Metal-Insulator Potential Barrier," J. Appl. Phys., 34, 490, (1963).

27. Geppert, D. V., "Experimental Determination of the Shape of Metal-Insulator-Metal Barriers," J. Appl. Phys. 35, 2151 (1964).

28. Chow, C.K., "Effect of Insulating-Film-Thickness Nonuniformity on Tunnel Characteristics," J. Appl. Phys. 34, 2599 (1963).

29. Chow, C. K., "On Tunneling Equations of Holm and Stratton," J. Appl. Phys., 34, 2490, Aug. 1963.

30. Dekker, A. J., Solid State Physics, p. 222, Prentice-Hall, Englewood Cliffs, N. J., 1956.

31. Papoulis, A., Probability, Random Variables and Stochastic Processes, p. 233, McGraw-Hill Co., New York, N. Y., 1965.

32. Jackson, J. D., Classical Electrodynamics, Chapter II, John Wiley & Sons, New York, 1963.

33. Frohlich, H., Theory of Dielectrics, Clarendon Press, Oxford, 1958.

34. Grissom, D. and Hartwig, W. H., "Dielectric Dissipation in NaCl and KCl Below 4.2 °K," J. Appl. Phys. 37, 4784 (1966).